Imaging in Prostate Cancer

2

Joel R. Wilkie, Aradhana M. Venkatesan, Vrinda Narayana, Patrick Hurley, and Patrick W. McLaughlin

Contents

2.1 Overview of Imaging Modalities in Prostate Cancer..... 26
2.2 Imaging in Prostate Cancer Diagnosis and Staging..... 28
2.3 Imaging in Prostate Cancer Treatment Decisions and Treatment Planning..... 30
2.4 Prostate and Surrounding Structure Anatomy on MRI..... 32
2.5 Imaging in Prostate Cancer Recurrence..... 52
2.6 Summary..... 58
References..... 58

J. R. Wilkie
Department of Radiation Oncology, University of Michigan, Ann Arbor, MI, USA
e-mail: jwilkie@med.umich.edu

A. M. Venkatesan
Section of Abdominal Imaging, Department of Diagnostic Radiology, The University of Texas MD Anderson Cancer Center, Houston, TX, USA
e-mail: AVenkatesan@mdanderson.org

V. Narayana · P. W. McLaughlin (✉)
Department of Radiation Oncology, University of Michigan, Ann Arbor, MI, USA

Department of Radiation Oncology, Providence Cancer Institute, Novi, MI, USA
e-mail: vrinda@med.umich.edu; mclaughb@med.umich.edu

P. Hurley
Division of Urology, Providence Cancer Institute, Novi, MI, USA
e-mail: patrick.hurley@ascension.org

A. A. Solanki, R. C. Chen (eds.), *Radiation Therapy for Genitourinary Malignancies*, Practical Guides in Radiation Oncology,
https://doi.org/10.1007/978-3-030-65137-4_2

2.1 Overview of Imaging Modalities in Prostate Cancer

- Common imaging modalities used in prostate cancer are summarized in Table 2.1.
- Primary tumor anatomy is best seen on multiparametric magnetic resonance imaging (mpMRI), with an example of a peripheral zone (PZ) tumor shown in Fig. 2.1. This figure also shows an apparent diffusion coefficient (ADC) map generated from the diffusion weighted image (DWI), and computer-aided detection (CAD) software applied to the dynamic contrast enhanced (DCE) image.
- The use of mpMRI is described in Version 2 of the "Prostate Imaging: Reporting and Data System (PI-RADS V2)," published in 2015 by the American College of Radiology, the European Society of Urological Radiology, and the AdMeTech Foundation in order to promote standardization in the acquisition, interpretation, and reporting of prostate mpMRI [1]. Several points of interest for the radiation oncologist regarding each imaging sequence are listed in Table 2.2.
- mpMRI is useful for identifying and classifying tumors confined to the prostate itself, and also has a central role in characterizing local disease extent: most importantly, determining whether the disease is confined to the gland (≤T2 disease) or not (≥T3 disease).

Table 2.1 Imaging modalities commonly used in prostate cancer

Imaging modality	Use in prostate imaging
Trans rectal ultrasound (TRUS)	Prostate localization during biopsy and brachytherapy procedures, both alone and with MRI fusion.
Computed tomography (CT)	Abdominopelvic scans are commonly used to assess locoregional disease and for radiotherapy treatment planning.
Multiparametric magnetic resonance imaging (mpMRI)	Evaluation of disease to help with biopsy and radiation or surgical treatment planning. Combines anatomic T2-weighted (T2W) images with functional and physiologic assessment provided by diffusion-weighted imaging (DWI) and dynamic contrast-enhanced (DCE) MRI. It provides visualization of locoregional anatomy, including prostate, regional lymph nodes, and surrounding critical structures.
Bone scan (BS)	Used for staging. Scintigraphic imaging that demonstrates increased metabolism suggestive of possible bone metastases.
Supersensitive positron emission tomography (PET)	Uses tumor-specific radiotracers to localize sites of disease in the soft tissues and/or bones. More commonly used in the setting of recurrent disease for restaging rather than at time of initial diagnosis. Currently, three are FDA approved (F-18 fluoride, C-11 choline F-18 fluciclovine), and others are being investigated.

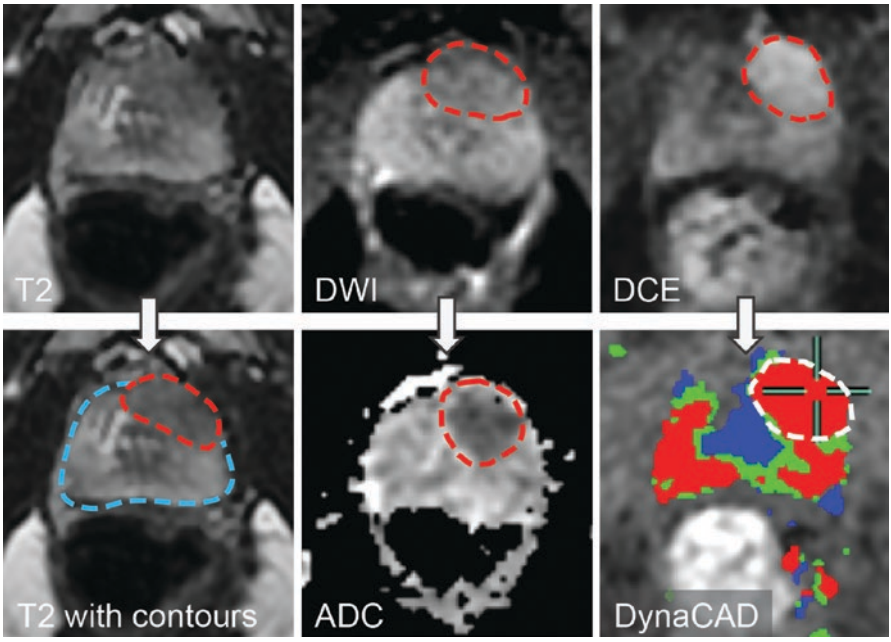

Fig. 2.1 Multiparametric MRI sequences. In this summary figure, all common sequences in use are depicted. In the absence of hemorrhage, tumor appears dark and nodular in the peripheral zone (PZ). Diffusion-weighted images (DWI) confirm the region as consistent with higher grade disease. The apparent diffusion coefficient (ADC), generated from DWI, confirms high grade disease. The dynamic contrast enhancement (DCE) scan reveals early uptake in tumor relative to the remaining normal peripheral zone. The CAD software applies an analysis to all DCE sequences to confirm rapid uptake and rapid clearance

- Typical MRI findings suggestive of extra-capsular extension (ECE) or seminal vesicle invasion (SVI) are summarized in Table 2.2.
- mpMRI is subject to inter-reader interpretation, while magnet strength and applied thresholds for defining ECE and SVI also lead to variability in sensitivity and specificity for identifying T3 disease. Specificity is typically higher than sensitivity, with pooled data from a meta-analysis showing sensitivity = 57% and specificity = 91% for ECE, and 58% and 97%, for SVI, respectively, compared to pathology from prostatectomy specimens [2].
- Specific examples of tumors at different sites within the prostate and the surrounding normal structures will be presented throughout the remainder of this chapter.

Table 2.2 Summary of PI-RADS 2 points of interest for the radiation oncologist

MRI sequence	*Notable uses*	*Typical tumor appearance*
T1 weighted (T1W)	Identification of hemorrhage: hyperintense signal in PZ and/or seminal vesicle (SV) following biopsy	Not part of PI-RADS scoring criteria
T2 weighted (T2W)	Driver for detecting clinically significant TZ cancers	Ill-defined hypointense focal lesions: TZ tumors commonly called "charcoal rub" Other features: spiculated margins, absence of complete hypointense capsule, invasion of urethral sphincter, and anterior fibromuscular stroma
Diffusion-weighted imaged (DWI)	Driver for detection clinically significant PZ cancers	Restricted/impeded diffusion, hypointense on ADC maps Conspicuity improved on high b-value images: hyperintense reflecting reduced diffusion
Dynamic contrast enhanced (DCE)	Can upgrade PZ PIRADS 3 tumors by DWI to PIRADS 4 Major use for recurrent tumors, especially post-RT	"Positive" lesion has focal enhancement, earlier or same time as that of adjacent normal prostatic tissues and corresponds to T2W and/or DWI
Staging criterion	*Preferred sequences*	*Typical findings*
Extra-capsular extension (ECE)	T2W Can be supplemented by high spatial resolution contrast-enhanced fat suppressed T1W	Asymmetry or invasion of neurovascular bundle (NVB), bulging prostatic contour, irregular or spiculated margin, obliteration of rectoprostatic angle, tumor–capsule interface >1.0 cm
Seminal vesicle invasion (SVI)	T2W DCE	Focal or diffuse low T2W signal intensity and/or abnormal contrast enhancement within and/or along the SV, restricted diffusion, obliteration of the angle between the base of the prostate and SV, and demonstration of direct tumor extension from the base of the prostate into and around the SV *Note: SVs often embedded within the prostate (wedged between TZ and PZ)*

2.2 Imaging in Prostate Cancer Diagnosis and Staging

- The role of imaging in the diagnosis of prostate cancer was historically limited to transrectal ultrasound (TRUS) for prostate localization during the initial biopsy procedure. TRUS continues to be used routinely for this purpose, and additional imaging is based on risk factors for more advanced disease.
- Development of more advanced imaging techniques has expanded the potential role of imaging to include early detection, improved diagnosis, and informed treatment decision-making.

2.2.1 Prostate Cancer Screening

- mpMRI has greatly improved the ability to visualize suspicious prostate lesions. It has a high sensitivity (58–96% in reported literature) for detecting Gleason ≥7 prostate cancer in a screening population, which translates to a high negative predictive value (63–99%) in this group [3–6].
- Several imaging sequences can be used in mpMRI but much of the information needed to detect both peripheral zone and transition zone lesions comes from T2-weighted (T2W) and diffusion-weighted MRI (DWI) sequences, which can be obtained relatively, rapidly and without contrast [7].
- mpMRI could have a future role in prostate cancer screening and may be particularly helpful for detecting high-grade cancers that are not associated with elevated Prostate-Specific Antigen (PSA) and responsible for 10% of prostate cancer mortality [8]. Prospective studies of MRI-based screening are in progress (Sunnybrook Health Sciences Center, NCT02799303).

2.2.2 MRI-Directed Biopsies

- Clinically significant prostate cancers can be missed with the traditional diagnostic approach (PSA, DRE, random TRUS biopsies). mpMRI with MRI/TRUS fusion-targeted biopsies offers a more focused approach with image-guided sampling of suspicious lesions.
- Published clinical trials have shown that MRI/TRUS fusion-targeted biopsies improve detection of clinically significant prostate cancers with fewer diagnoses of insignificant cancers compared to the standard sextant biopsy approach [9]. These data imply that mpMRI is better at visualizing high-grade cancers and less sensitive for low-grade cancers. In addition, MRI/TRUS fusion-targeted biopsies missed about 10% of high-grade cancers that were detected by traditional random TRUS biopsies.
- More efficient and less costly mpMRI has the potential to offer a high clinically significant cancer diagnosis rate with few false negative cases [10]. MRI can also be used for regional lymph node assessment; meaning, diagnostic CT scan is not necessary if MRI is acquired.
- Given the management implications of higher-grade prostate cancer, we routinely obtain mpMRI prior to discussing treatment options and recommendations, including active surveillance, unless contraindicated.

2.2.3 Exclusion of Metastasis

- National Comprehensive Care Network (NCCN) guidelines recommend obtaining a CT or MRI of the abdomen/pelvis if the nomogram-predicted chance of positive pelvic lymph nodes is greater than 10% [11].

- Bone scan is recommended for symptomatic patients, those with high risk prostate cancer or unfavorable intermediate risk disease with clinical stage T2 and PSA >10 ng/mL.
- Standard positron emission tomography (PET) scans using ^{18}F-fluorodeoxyglucose (FDG) (^{18}F-FDG) should not be used for routine prostate cancer staging.
- ^{18}F sodium fluoride PET-CT has greater sensitivity but lower specificity than radionuclide bone scan [12], and given its unproven effect on oncologic outcomes and implications of a positive study, the NCCN only recommends consideration of its use for evaluation of equivocal findings on bone scan [9].
- Other types of supersensitive PET scans (e.g., ^{11}C/^{18}F choline, ^{18}F fluciclovine and ^{68}Ga/^{18}F PSMA) are not currently recommended for the upfront staging of prostate cancer.

2.2.4 Characterization of Metastatic Disease

- With the interest in tailoring treatment of metastatic prostate cancer based on disease burden, the role of supersensitive PET is likely to expand in the near future.
- Multiple recent trials have suggested a differential benefit of various treatment strategies between patients with low-burden metastatic disease or oligometastatic disease (commonly defined as up to three bone metastases without visceral metastases) compared to high-burden metastatic disease [13, 14]. Distant staging in these studies was based on bone scans, and it is possible that the survival benefit of treating patients with oligometastatic disease with local ablative therapies could be even more pronounced if supersensitive PET imaging were used.
- The European Organization for Research and Treatment of Cancer's (EORTC) Imaging Group recently recommended a clinical trial design in which patients with high risk prostate cancer and negative bone scan are randomized to use of a modern imaging method (supersensitive PET) or not, to determine the treatment approach [15]. Although some clinicians favor discussion of the risks and benefits of supersensitive PET imaging in this scenario, its use is not recommended in current guidelines.

2.3 Imaging in Prostate Cancer Treatment Decisions and Treatment Planning

2.3.1 Functional Anatomy at Consultation to Predict Quality of Life Outcomes After Treatment

- Improved imaging of the prostate, prostate tumors, and the local anatomy involved in normal genitourinary (GU), gastrointestinal (GI), and sexual function provides information that is useful for treatment selection.

- Extra-capsular extension and/or seminal vesicle invasion predict a higher likelihood of needing post-operative radiotherapy for patients considering radical prostatectomy [16, 17].
- Short external urethral sphincter (less than 0.5 cm) suggests a higher probability of long-term urinary incontinence following prostatectomy [18]. It is critical to recognize men with a long external sphincter as this predicts low risk of incontinence with surgery. In radiation planning, recognizing the long sphincter drastically limits prostate overestimation and decreases the risk of strictures, which are a function of sphincter length exposed.
- Identification of the neurovascular bundles (55%) versus plexus (40%) versus absent (5%) on MRI can help to predict the ability to spare the nerves at surgery and the type of operation necessary to accomplish preservation [19]. This may also allow dose restriction as some nerve elements extend >1 cm beyond the prostate.
- Understanding of local MRI anatomy helps to clarify the above issues and the associated tradeoffs and challenges in treatment decisions. It allows a neutral advocacy approach based on objective prediction of critical outcomes prior to therapy.

2.3.2 Imaging in Radiation Planning

- Accurate delineation of the prostate, required for ensuring tumor coverage while minimizing normal structure doses, is challenging on computed tomography (CT) scans.
- We have previously shown errors of both overestimation and underestimation at the base and the apex on CT when compared to MRI [20, 21]. Another study showed average prostate volume overestimation of 30% compared to the gold standard from the Visible Human Project, but with only 84% of the gold standard prostate volume included within the overestimated contours [22]. Critically in this study, the tumor-bearing peripheral zone was commonly underestimated.
- Experience with mpMRI and its availability in the planning process can rectify many contouring uncertainties. However, MRI to CT registration is often prone to registration uncertainties, and mpMRI scans are not always available; pacemakers and defibrillators make acquisition more difficult and dependent on cardiology support.
- Familiarity with MRI anatomy and common CT contouring errors is valuable in mitigating uncertainties leading to over- and underestimation of the prostate volume [20].
- Common pitfalls in interpreting mpMRI images must be avoided in the treatment planning process [23].
- In the following sections, we review prostate and surrounding structure anatomy and discuss important variant anatomy, functional anatomy, tumor anatomy, and dynamic anatomy as appropriate.

2.4 Prostate and Surrounding Structure Anatomy on MRI

2.4.1 General Prostate Anatomy

- Substructures of the prostate are best seen on T2W imaging in which the central zone (CZ) and transition zone (TZ) demonstrate low signal, while the larger peripheral zone (PZ) has high signal that is generally similar to or greater than adjacent periprostatic fat (Fig. 2.2).
- Much of the variability in prostate size and shape is due to the increasing size of the transition zone due to benign prostatic hyperplasia (BPH).
- The prostate "capsule" is a dark rim of low signal on T2W and is composed of concentric fibromuscular tissue that surrounds the peripheral zone (pseudocapsule) rather than a true capsule.
- The anterior fibromuscular stroma (AFMS) is a low signal dense fibrotic band anterior to transition zone and extending down over the anterior peripheral zone near the apex, often merging with the external sphincter.
- The prostatic "surgical capsule" is composed of compressed prostate tissue that appears as a thin dark rim at the interface of the transition zone and peripheral zone on T2W [24].
- The seminal vesicles (SVs) consist of regions of alternating high and low signal corresponding to seminal fluid and walls, respectively.
- The distal urethra is a low intensity circular structure that extends through the genitourinary diaphragm (GUD).

2.4.1.1 Zonal Anatomy

- The most striking difference between CT-based and MRI planning is the clear definition of the peripheral zone versus the transition zone and central zone (Fig. 2.2). Most tumors arise from the peripheral zone. A common contouring error in the enlarged gland on MRI is to contour the transition zone as prostate, ignoring the rim of peripheral zone compressed by transition zone enlargement.

2.4.1.2 Dynamic Anatomy

- Transition zone hypertrophy is responsible for benign prostate enlargement but ADT treatment reduces peripheral zone volume on average greater than transition zone [25].
- External beam radiation alone preferentially diminishes peripheral zone volume more than transition zone [26]. This in part explains the greater challenge of diagnosing recurrence after treatment.
- MRI and CT under different conditions of bladder and rectal filling make it clear that the prostate is highly deformable (Fig. 2.3).
- Deformability of prostate is directly apparent with TRUS brachytherapy procedures. The tension between a close probe, with a compressed but clear image versus a distant probe, with a less compressed, less clear image may favor the compressed probe. However, such compression may lengthen and widen the prostate shape relative to its native state as seen on MRI.

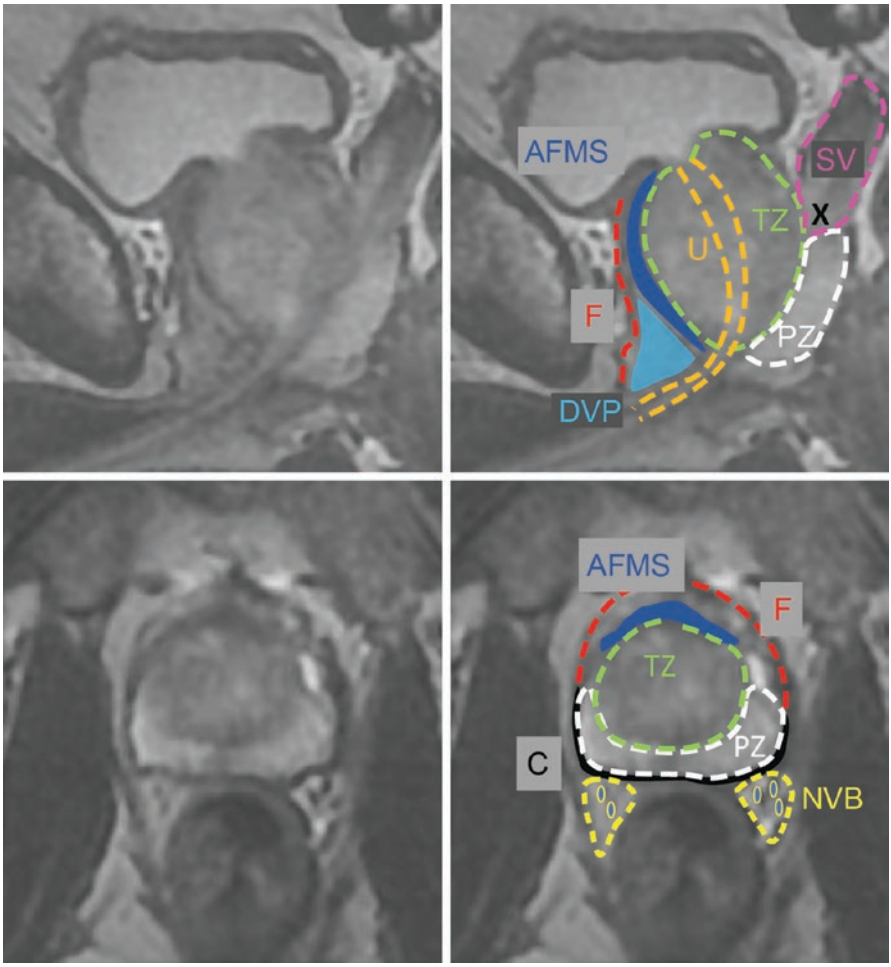

Fig. 2.2 Zonal anatomy, T2W sagittal and axial views. The darker transition zone (TZ) is distinct from the light peripheral zone (PZ). Note the relationship of the seminal vesicle (SV) to the TZ and PZ, embedded in the space between. The capsule (C) is distinct as is the anterior fibromuscular stroma (AFMS). The Neurovascular bundles (NVBs) are in classic posterior lateral position. The dorsal venous plexus (DVP) is highly variable within the fascia (F). Not pictured on these images, the central zone surrounds the ejaculatory ducts and is located posterior to the transition zone and the urethra proximal to the verumontanum

- Registration of MRI for fusion biopsies and brachytherapy to a compressed prostate requires considerable deformation. Brachytherapy done under compression may have the radioactive source distribution completely altered in unpredictable ways when the probe is removed, the so called "Bermuda Triangle" effect [27].

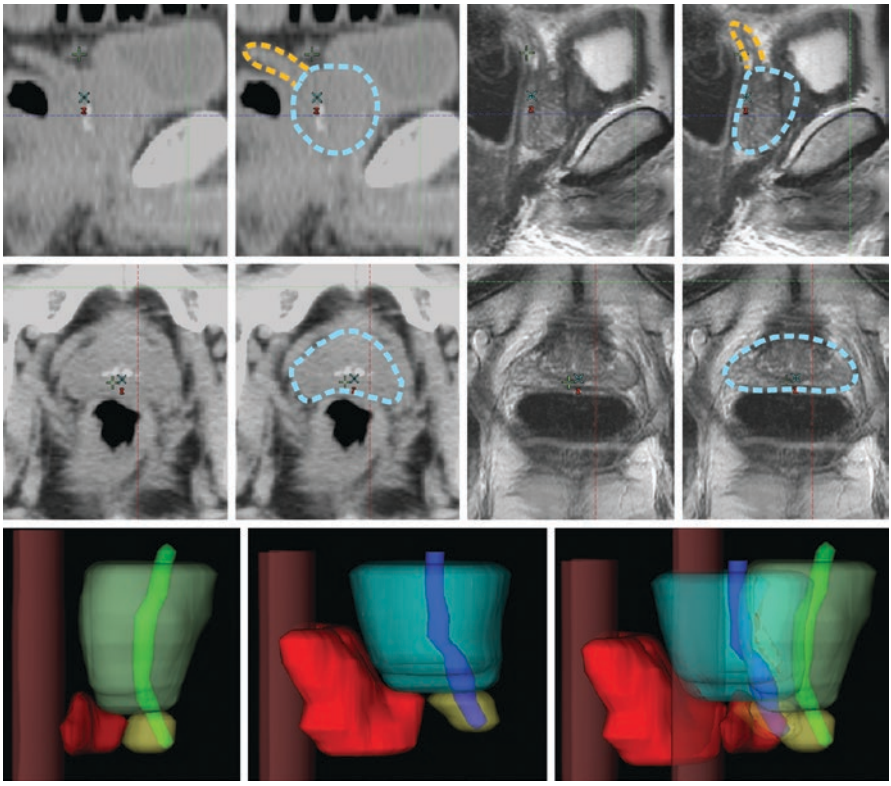

Fig. 2.3 Prostate deformation. The upper and middle panels show the prostate compressed on MRI imaging by rectal expansion with volume preservation. Note the decreased AP distance and increased lateral distance relative to the CT. In the lower panels, the left image is a 3D reconstruction of a prostate with probe close/compressing. The middle panel is the same prostate with the probe relaxed (dropped inferior). Note the prostate is shorter and wider with the relaxed probe. The rectourethralis muscle (red) fans out dramatically. On the right is image overlay. Note there is greater mobility at the base than the apex due to relative fixation of the urethra in the GU diaphragm

2.4.2 Apex Anatomy

- The apex is exclusively peripheral zone, and as such has a high risk of tumor. The apex and sub-apex are also responsible for the most devastating chronic treatment complications including stricture and rectal ulcer and fistula.
- Clear definition of the apex on imaging can help prevent unnecessary delivery of dose to uninvolved external sphincter, particularly for brachytherapy, in which very high doses beyond the apex can increase the late urinary toxicity rate without contributing to cure of the disease [28].

2.4.2.1 Variant Anatomy

- The external sphincter commonly extends within the prostate (Fig. 2.4), with the extent varying from approximately 0.5–1.5 cm [29]. This creates the greatest oncologic challenge to cure and QOL in the prostate region: dose escalation of the peripheral zone at the apex will inevitably dose escalate a portion of the external sphincter.
- The extent of external sphincter projection within the prostate is clearly visualized on T2W MRI images, and the apex limit is clearly defined on coronal views or through the use of genitourinary diaphragm recognition (see below).

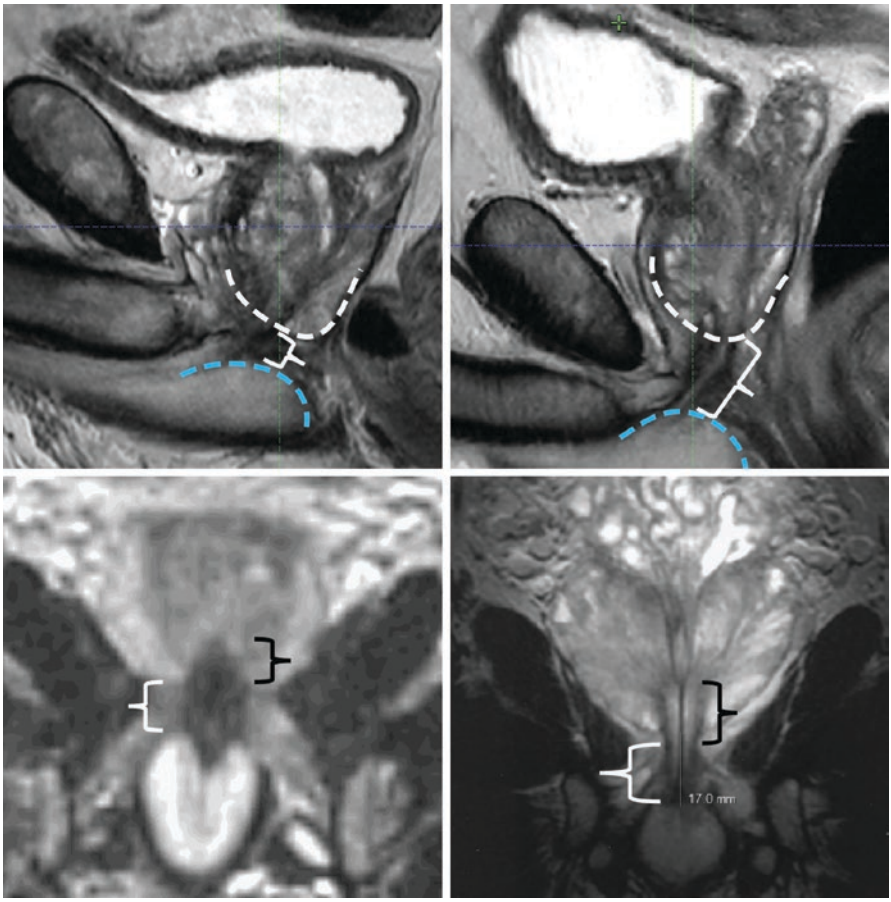

Fig. 2.4 External sphincter variants. In the left upper panel, note the prostate apex lies in the pelvis well below the symphysis, and the external sphincter is very short (<1 cm). In the right upper panel, the external sphincter is longer and the apex lies just above the symphysis. Variable extension within the prostate is depicted in the lower panels, with minimal extension in the left panel, and >1 cm extension within the prostate in the right panel

2.4.2.2 Dynamic Anatomy

- A key advantage of a distant, less compressed TRUS position is a dramatic change in prostate apex shape, from a pointed tip with compression to a flat face perpendicular to the needle direction during brachytherapy.

2.4.2.3 Tumor Anatomy

- Tumor recognition at the level of the peripheral zone at the apex is easier than within the transition zone. Tumor appears on T2W imaging as a focus of low signal intensity (Fig. 2.5) in contrast to hemorrhage, which is typically less distinct and associated with corresponding increased signal on T1-weighted imaging.
- Diffusion and ADC are sufficient to suggest Gleason 7 or higher lesions.
- Extension of tumor into the neurovascular elements (NVEs) or plexus is a critical consideration for surgery and radiation therapy planning.

2.4.3 Seminal Vesicle Involvement

- Although schematic depictions of the seminal vesicles present them as a leaf on a stalk, MRI sagittal views demonstrate the embedding of seminal vesicles in the notch between the peripheral zone and transition zone (Fig. 2.2).
- Evidence suggests that SVI directly from the prostate through the ejaculatory duct complex may not have the same implications as SVI from extra-capsular extension of disease outside the prostate extending to the seminal vesicles [30].

2.4.3.1 Functional Anatomy

- SVI is more easily seen when the seminal vesicles are full. Abstinence for 3–5 days prior to the MRI improves seminal vesicle assessment.
- The ejaculatory ducts pass through the prostate just lateral to the urethra, terminating at the verumontanum. Peripheral weighted brachytherapy plans may lead to less disruption of the thin duct as part of an ejaculation sparing strategy.

2.4.3.2 Tumor Anatomy

- Figure 2.6 shows an example of normal seminal vesicle anatomy along with T2W and DWI MRI images of SVI.
- mpMRI manifestations of SVI are listed in Table 2.2, and many are evident in Fig. 2.7, in which much of the seminal vesicles are involved. These findings are not always present, particularly for microscopic SVI, leading to a relatively low average sensitivity of 58% in one meta-analysis (although some studies did not include functional MRI sequences [2]).

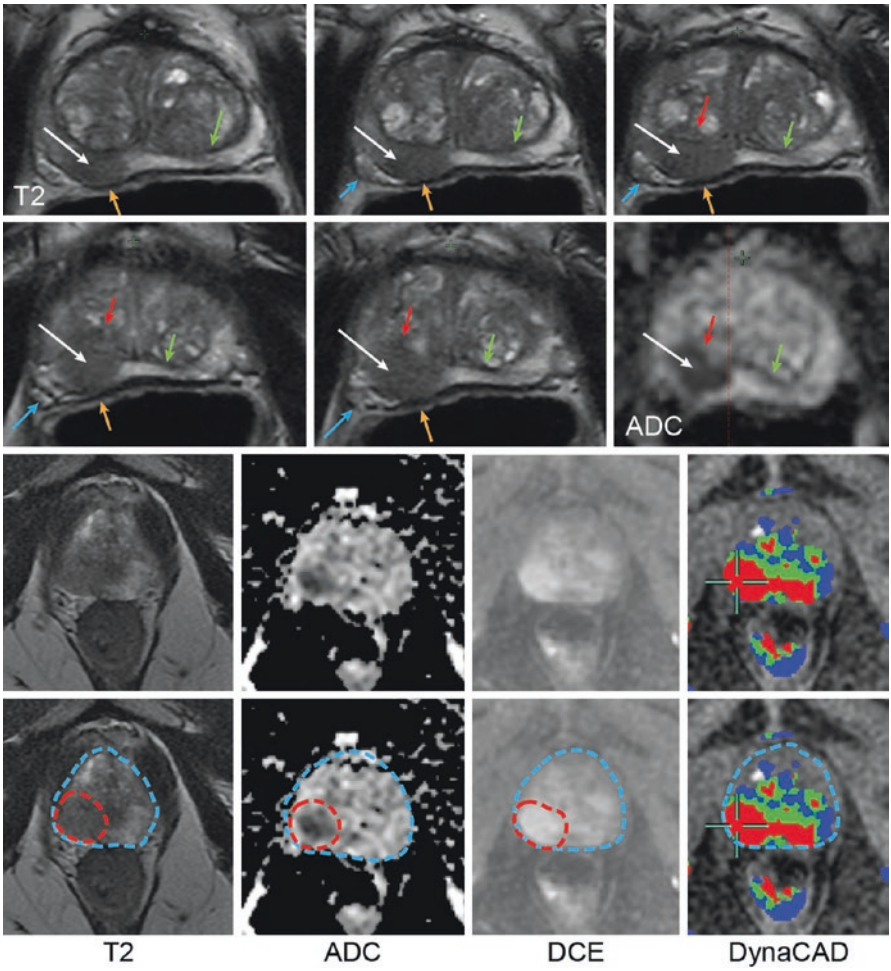

Fig. 2.5 Tumor recognition in the Peripheral Zone (PZ). Note the exquisite detail provided by T2W. The normal PZ is light and the left PZ (screen right) is light and homogeneous without evidence of tumor. Tumor appears as a discrete dark nodular area in the right lobe (white arrows). Again the complex reticular and cystic TZ contrasts with the homogeneous PZ. Note the tumor expands the lobe but does not disrupt the capsule (yellow arrows) and does not invade or efface the neurovascular bundle (blue arrows). Note how the tumor has invaded the TZ, with effacement of the internal capsule (red arrows). An intact internal capsule is present on the left (green arrows). In the lower panels, a peripheral nodule is depicted on mpMRI sequences. The diffusion and ADC sequence positivity implies the dark area is equal to at least Gleason 7 disease. The DCE depicts rapid uptake by tumor (unlike TZ normal PZ takes up contrast late) and the Dynacad analysis confirms both rapid uptake and rapid clearance consistent with tumor. Prostatitis has increased uptake but not rapid clearance

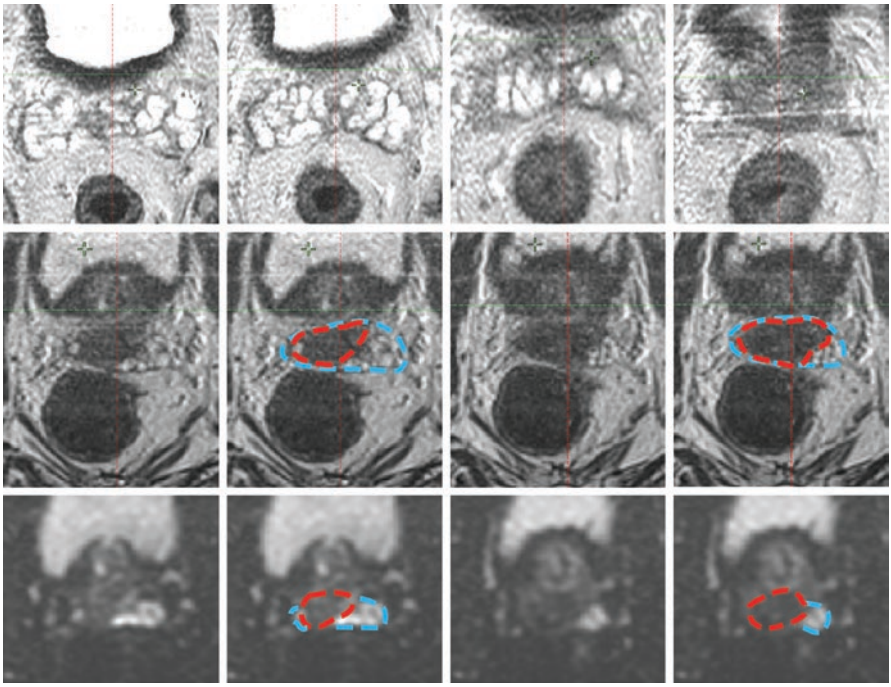

Fig. 2.6 Seminal vesicle involvement. The upper panels show normal appearance of cystic seminal vesicles. Abstinence is recommended for 3 days prior to diagnostic scan. In the middle panels, the tumor (red) effaces the cystic architecture with some normal structure visible (blue). In the lower panels, DWI sequence clearly defines the tumor and normal adjacent SV

- mpMRI predicts SVI from prostatectomy specimens better than the Partin [31] tables alone, and combining Partin tables and mpMRI improves this performance [32].
- Direct MRI visualization solves one of the controversies regarding treatment planning and seminal vesicle sparing: extent of seminal vesicle involvement. SVI beyond the proximal 2 cm is rare [33], and distal SVI almost never occurs without proximal SVI [34].
  - Sparing the middle and distal seminal vesicles from high doses of radiotherapy could allow for preservation of ejaculate. Direct imaging of involvement improves the accuracy, but given that SVI is not infrequently documented in the absence of MR evidence, there is concern that relying solely on MRI for volume delineation could miss cancerous cells in some instances.
  - When an expert genitourinary radiologist reviewed mpMRI for SVI in a recent study, only 1 case of SVI extending beyond the base of the seminal vesicle was missed from a total of 41 cases of SVI detected on prostatectomy specimens [32].

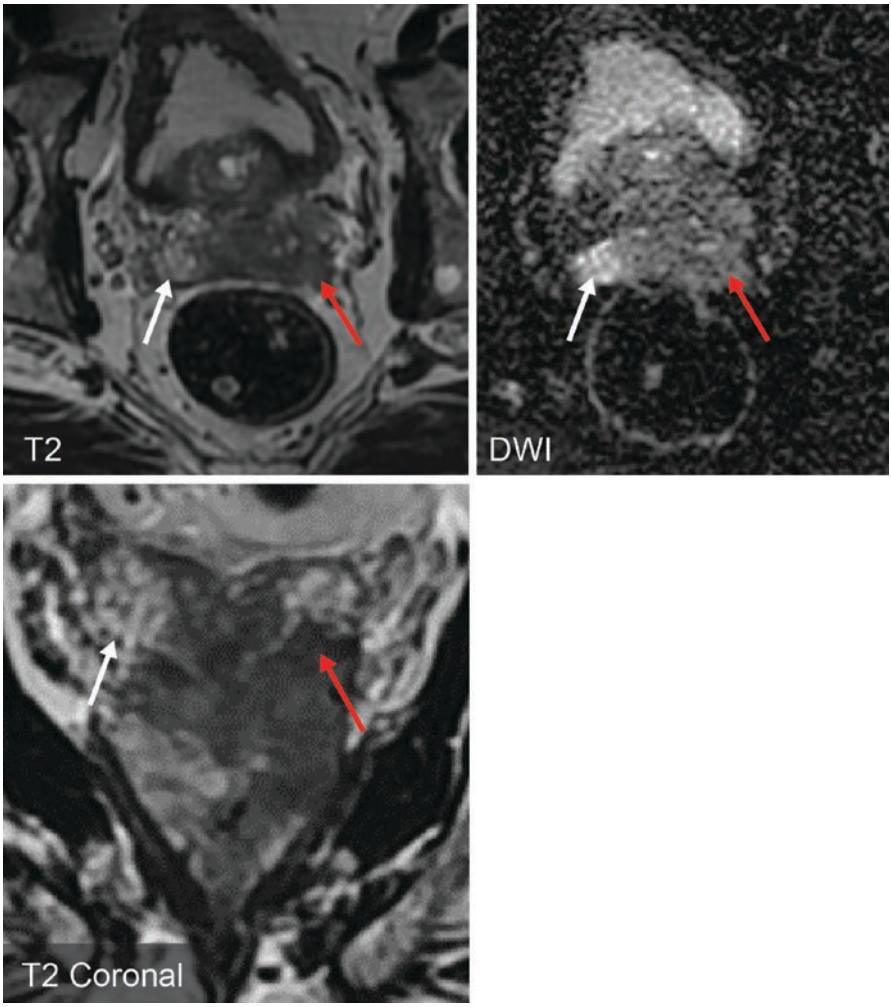

Fig. 2.7 Additional seminal vesicle involvement. In the T2W axial, there is clear infiltration of the seminal vesicle confirmed (red arrow). On DWI and T2W coronal, normal SV is preserved in non-involved regions (white arrows)

2.4.4 Extra-capsular Extension

- Extra-capsular extension can often be detected on mpMRI and is a critical factor influencing treatment selection. Studies have demonstrated relatively lower sensitivities (0.49–0.58) and higher specificities (0.82–0.98) for extra-capsular extension on mpMRI [2, 35, 36]. These may be highly dependent on the expertise of the reader, threshold used for defining ECE and magnet strength. Positive predictive value has been shown to depend on risk group [36].

  - An initial meta-analysis suggested that the use of endorectal coils improved the staging performance for extra-capsular extension [37]; however, a more recent meta-analysis showed that sensitivity was improved by using functional imaging in addition to T2W, and by use of 3 T field strengths, but not by use of endorectal coils [2]. At our institution, we obtain mpMRI using 3 T MRI without endorectal coil.
  - A recent single institution analysis showed improvement in models to predict extra-capsular extension by adding mpMRI to those using Partin tables alone [38].
- Common findings of extra-capsular extension on mpMRI are listed in Table 2.2, and example images are shown in Fig. 2.8.

2.4.5 Base Anatomy

- The base refers to the superior prostate, located in contiguity with the urinary bladder. This is the *most dynamic* anatomic region in the long term, as over decades the transition zone may enlarge due to benign prostatic hyperplasia, expanding the bladder neck, and ultimately effacing the bladder neck and extending within the bladder lumen.

2.4.5.1 Variant Anatomy

- The stepwise, progressive variants shown in Fig. 2.9 are intact bladder neck (class I), expanded bladder neck (class II), effaced bladder neck with limited bladder penetration (class III), and full bladder lumen penetration with or without a median lobe (class IV) [39].
- Most acute urinary toxicity is attributed to radiation dose at the prostate base and the transition zone is generally at low risk (24%) of cancer involvement [40]. It is possible that sparing the base from the highest doses of RT could improve treatment tolerability without decreasing the likelihood of disease control.
- The bladder neck is best visualized on T2W sagittal MRI images (Fig. 2.9a) but can also be seen on axial MRI and TRUS (Fig. 2.9b).

2.4.5.2 Functional Anatomy

- In spite of extreme variation in size, shape, and bladder extension of the prostate, it is not possible to predict bladder function from MRI anatomy. Some men with markedly enlarged glands and even median lobe do not have restriction of urine flow.
- Most acute urinary toxicity during therapy is bladder-neck related, with common symptoms including dysuria as urine is forced through a restricted, inflamed channel, and pain referred to the tip of the penis. The majority of the time such burning and referred pain is not related to infection and is fully relieved by alpha blockers plus non-steroidal anti-inflammatories.

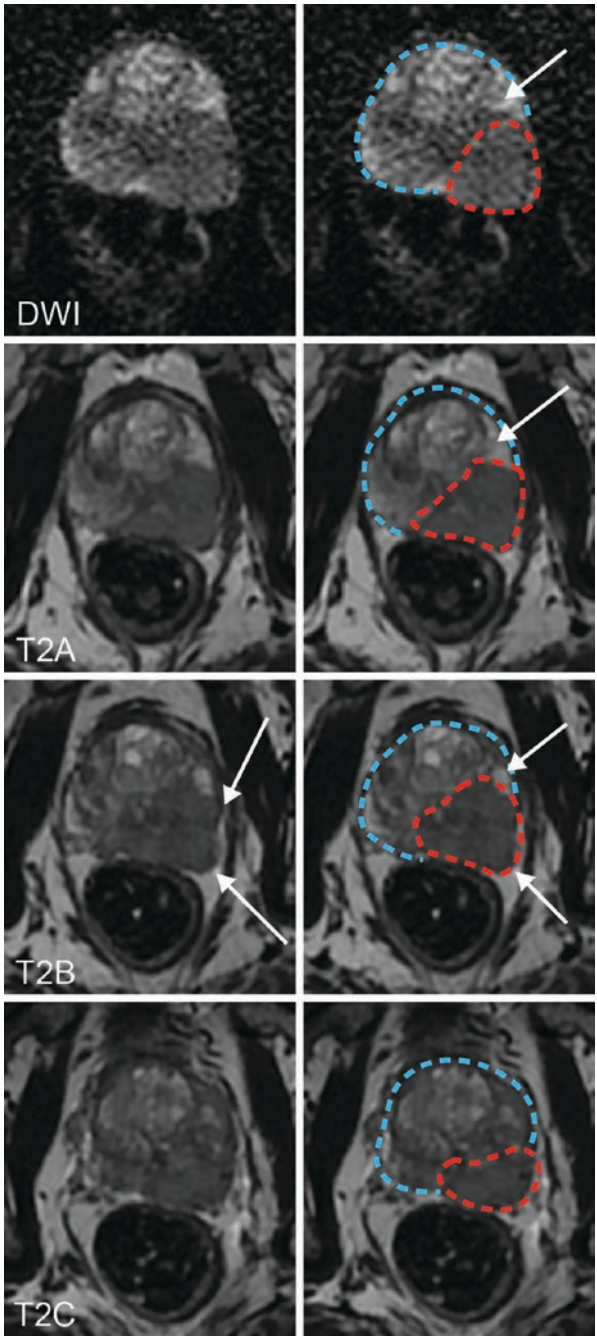

Fig. 2.8 Extracapsular extension (ECE). In these scans, there is a strong suggestion of capsule disruption. In the DWI (top panels), there is evidence of a step off where the tumor appears to breach the capsule. In the T2W images (T2A, T2B, T2C), the outer contour has a nodularity (white arrows) rather than a smooth expansion appearance

- Alpha blockers work by opening the restriction point at the bladder neck. A non-urinary sequel of alpha blockers is retrograde ejaculation. Dose escalation at the bladder neck may result in a life-long requirement for alpha blocker therapy, precluding ejaculation sparing.

2.4.5.3 Tumor Anatomy

- Recognition of transition zone tumors is more difficult than peripheral zone tumors due to its relative hypointense signal on T2W imaging that can overlap visually with the signal intensity of prostate cancer and the heterogeneous appearance of transition zone in the setting of benign prostatic hyperplasia. Optimal Tumor assessment and recognition under specific circumstances (anatomic zone, post radiation, and post surgery) is summarized in Table 2.3.
- Cancers within transition zone typically appear as areas of low signal on T2W imaging and ADC associated with ill-defined margins described as having an "erased charcoal" appearance (Fig. 2.10). DWI and ADC findings should corroborate the abnormality seen on T2W imaging.
- Excluding tumor at the bladder neck allows bladder neck sparing with brachytherapy applications but is not technically possible with external beam gradients.

2.4.5.4 Dynamic Anatomy

- Maintaining bladder filling may allow exclusion of 80% of the bladder volume, but as irritation proceeds during the treatment course, this may be increasingly difficult. The goal is for the bladder to be as full as possible without being so full that urgency ensues during the treatment.

2.4.6 Genitourinary Diaphragm

- The genitourinary diaphragm extends from the prostate apex to the penile bulb, and the external sphincter courses throughout.

2.4.6.1 Variant Anatomy

- Genitourinary diaphragm anatomy can vary widely, with external sphincter length ranging from approximately 0.5 to 3.5 cm in length (Fig. 2.4).
- Defining the genitourinary diaphragm and its layers is distinct on MRI (Fig. 2.11), and once trained in MRI it is possible to recognize these levels (bulb, triangle, circle, hourglass, apex) on CT to avoid overestimation at the apex [20].

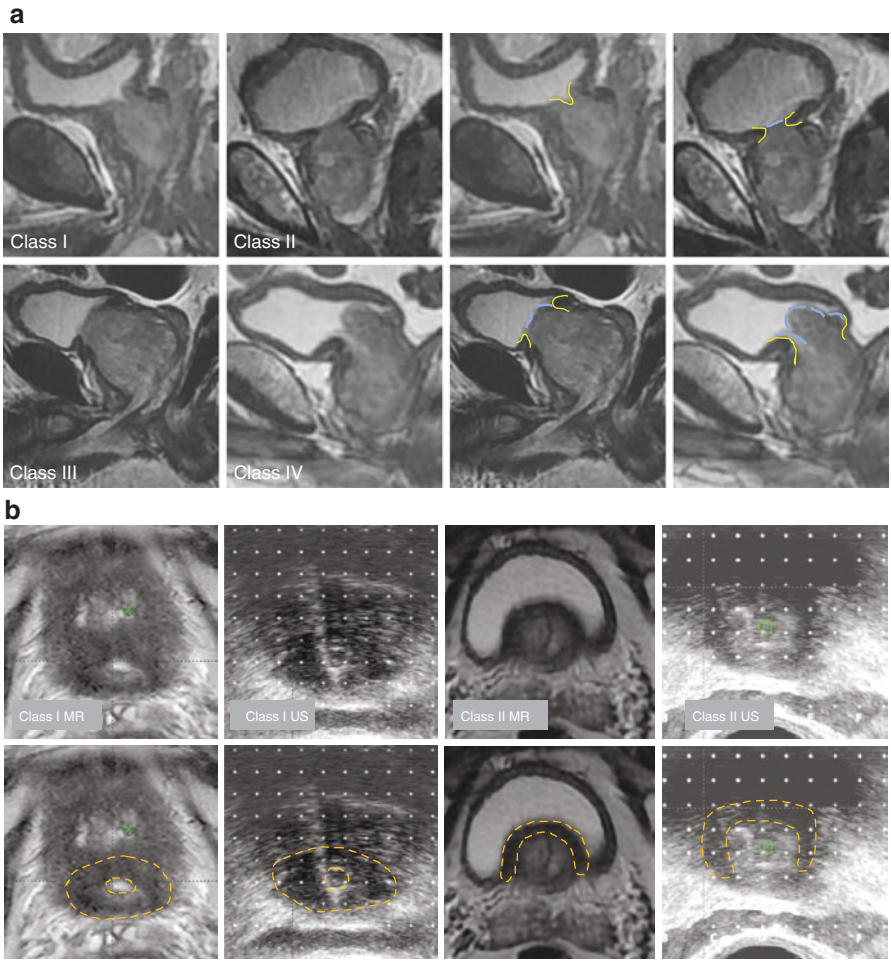

Fig. 2.9 Base Variants: (**a**) Sagittal MRI depicting the four class system for base variants. Class I (bladder neck intact), Class II (Bladder neck expansion), Class II (Projection of prostate into the bladder lumen), and Class IV (median lobe or asymmetric hypertrophy). In (**b**) axial MR and US both clearly depict Class I and Class II involvement at the bladder neck. The US does not depict the actual bladder lumen as clearly as the MRI due to distance from the probe

Table 2.3 Best imaging options (modality or mpMRI sequence) for specific circumstances

Circumstance	Primary sequence or modality	Secondary sequence or modality
TZ tumor	T2W with "charcoal smudge"	DWI
PZ tumor	DWI with restricted/impeded diffusion	DCE with rapid focal enhancement
Recurrence post-RT	DCE with rapid focal enhancement	DWI; consider supersensitive PET
Gross recurrence post-RP	T2W for gross disease; DCE to distinguish from fibrosis	DWI; consider supersensitive PET

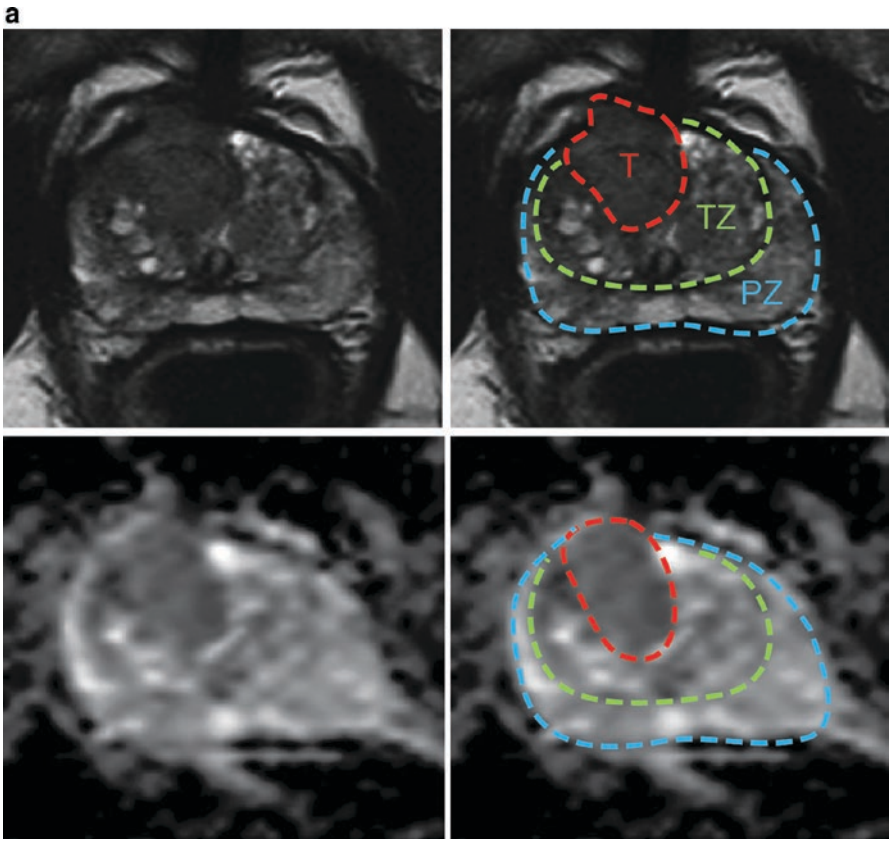

Fig. 2.10 Tumor recognition in the transition zone (TZ). The TZ has a complex reticular, lattice-like appearance compared to the relatively homogeneous peripheral zone. The TZ takes up contrast, limiting the value of contrast uptake in tumor recognition. Tumor can be recognized on T2W by the "erased charcoal" appearance which interrupts the reticular pattern. This is seen in (**a**) with T2W in the upper panel and ADC in the lower panel. In (**b**), an extensive high grade tumor extends from the PZ into the TZ (converse is possible). The tumor is recognized on all sequences but again the tumor effaces the complex reticular lattice pattern

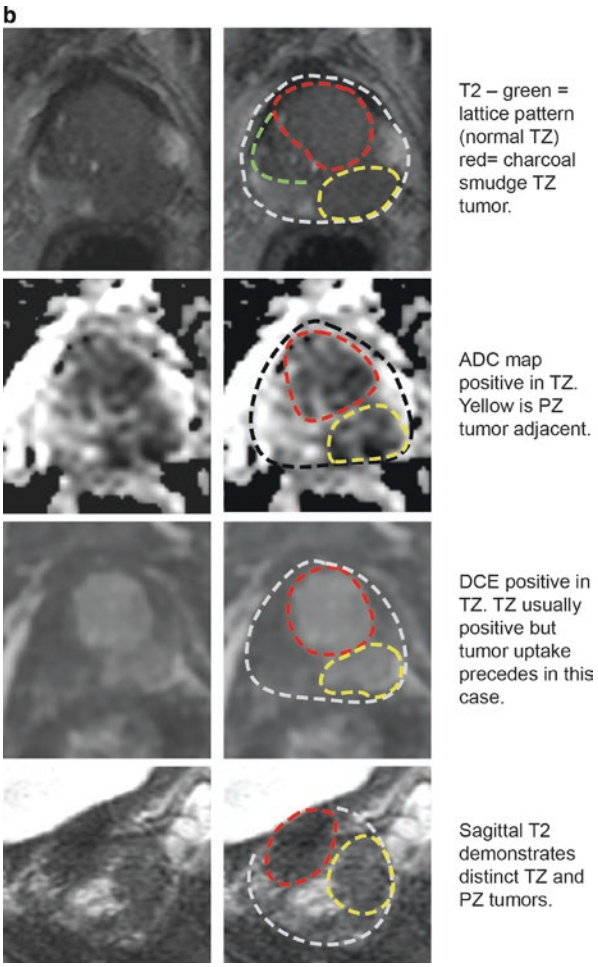

Fig. 2.10 (continued)

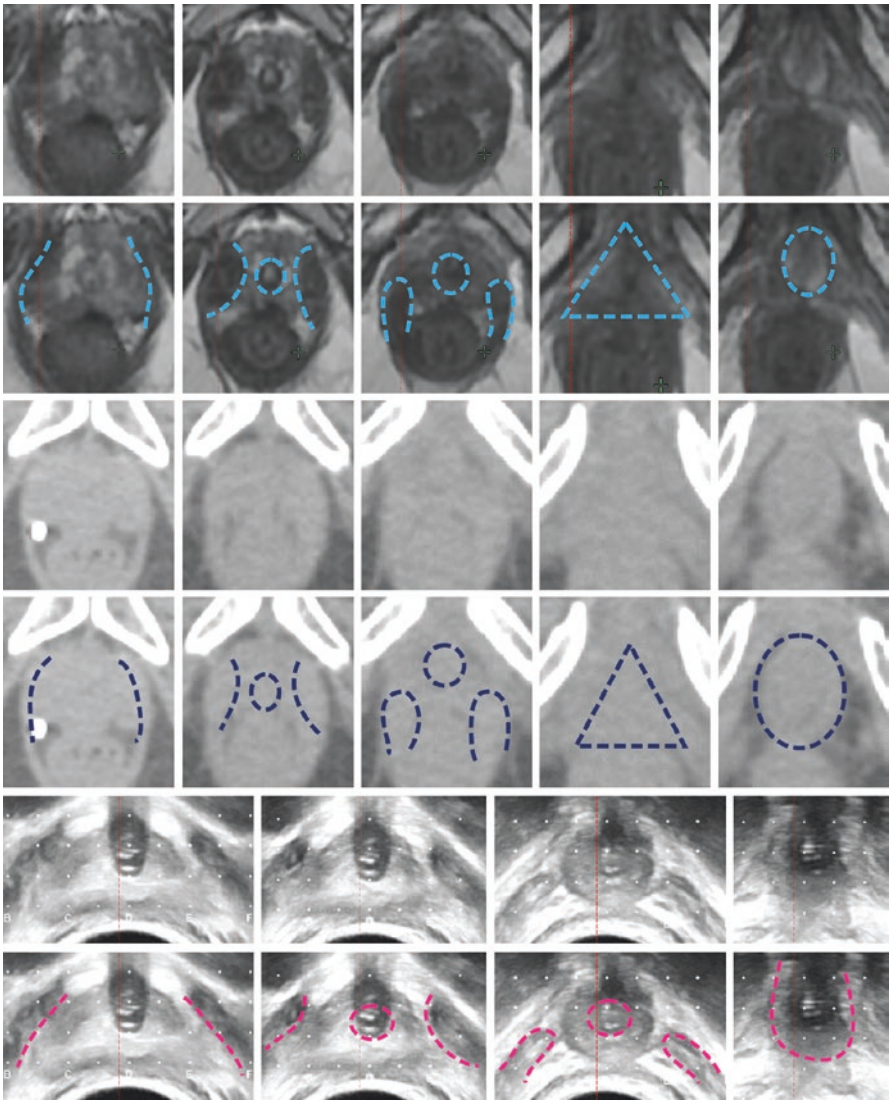

Fig. 2.11 Genitourinary diaphragm (GUD) recognition. Moving inferior from the apex are distinct patterns within the GUD. These patterns are very clear on MRI (upper two rows) but can often be recognized on CT (middle two rows) and US (lowest two rows), limiting both overestimation and underestimation at the apex. At the apex, the levator ani (LA) is concave, supporting the prostate. At the sub-apex, the LA is convex with the external sphincter in between. In the lower GUD the external sphincter is superior to the LA, the so-called "gold medal pose." A triangular area of relative homogeneity follows above the penile bulb

- Contouring rules based on average genitourinary diaphragm anatomy should be avoided. The 1.5 cm rule, suggesting the apex can be defined at 1.5 cm above the penile bulb, will grossly overestimate the apex in men with long external sphincter and grossly underestimate the prostate in men with short external sphincter.

2.4.7 Rectourethralis (RU)

- A critical structure in maintaining the ano-rectal flexure is the rectourethralis muscle (Fig. 2.12). This originates in the rectal wall and may appear merged with the rectum for much of its course until inserting on the genitourinary diaphragm and perineal body.
- Rectourethralis is recognized in some patients as a subtle thickening of the rectum at the genitourinary diaphragm level with a linear extension to the external sphincter and perineal body at its termination. It is commonly mistaken for rectal wall.

2.4.7.1 Dynamic Anatomy

- Rectourethralis anatomy is clearly affected by rectal TRUS probe position during brachytherapy procedures. When probe is placed, the rectum (normally held adjacent to the apex and genitourinary diaphragm by the rectourethralis) is pulled away, and the separation of the rectum and rectourethralis can be directly visualized on TRUS (Fig. 2.12b).
- There is an advantage in HDR of treating with a probe in place to exclude the rectum—most of the rectum is held >1 cm from the prostate.
- Anatomy is also critical to hydrogel spacer placement (Fig. 2.12d). Ideally the gel is placed above the rectourethralis, with less ideal placement being between the rectourethralis and rectum. Having the legs less extended can lessen the approach angle between the prostate and rectum/rectourethralis, improving spacer placement.

2.4.8 Sexual Preservation

2.4.8.1 Functional Anatomy

- Corpus cavernosa, critical end organs for erection, are situated below the genitourinary diaphragm, the most distal OARs affected by radiation.
- Surgical sexual function preservation is based on preserving the nerves through nerve sparing prostatectomy [41, 42], while sexual preservation after radiation

has no clearly defined single target [43–45]. Controversy remains as dose correlation studies have been based on inaccurate anatomic definition of critical sexual OAR.

- It is clear that when distal end organ and sub apex dose is limited (vessel sparing), excellent preservation of function is accomplished according to patient

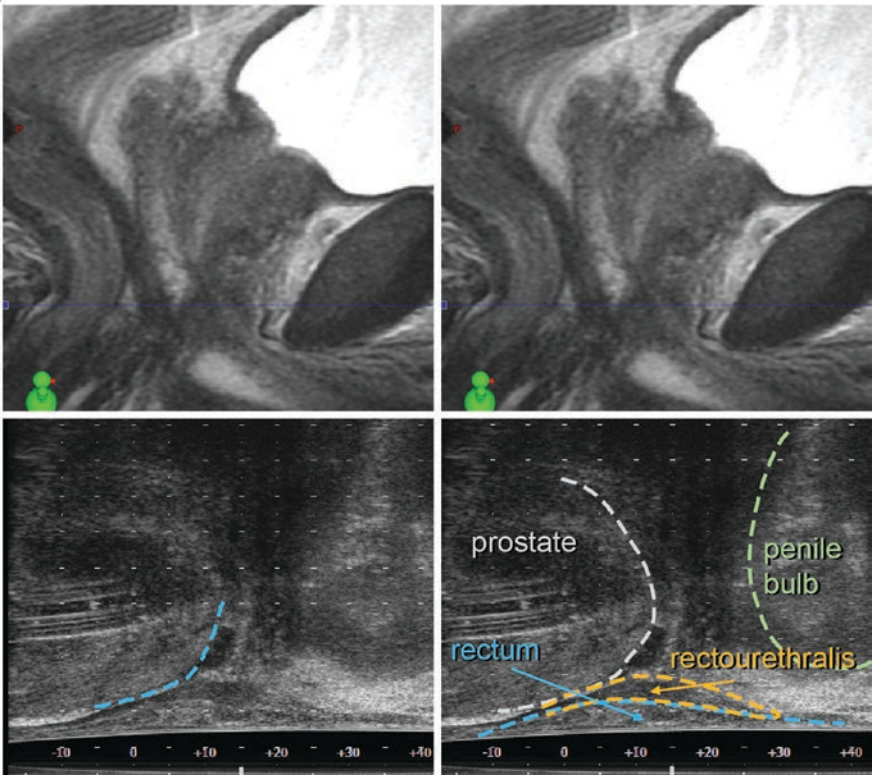

Fig. 2.12 Rectourethralis (RU) and rectum (R) dynamic anatomy. The RU is a distinct muscle often mistaken for rectal wall. It emanates from the rectal wall and connects to the GUD and is in part responsible for mainlining the recto-anal flexure or bend in the rectum between the storage and evacuation (anal) segment. (**a**) An unusually clear and substantial RU courses along the rectum and the inferior GUD and terminates near the perineal body. In the second row, an US sagittal view depicts the two layers (RU and R) adjacent. (**b**) As an US probe is pulled down away from the prostate, the layers are separated, with the tension causing both RU and R to fan out (recall Fig. 2.3). (**c**) One sees a very distinct RU extending along the prostate on MRI. This full length anatomic variant may complicate hydrogel spacer placement. For some patients, the gel tracks within the space between the RU and R, incorrectly described as within the rectal wall. Ideally the gel is above the RU and below the prostate. (**d**) Both gel placement patterns are depicted and are acceptable

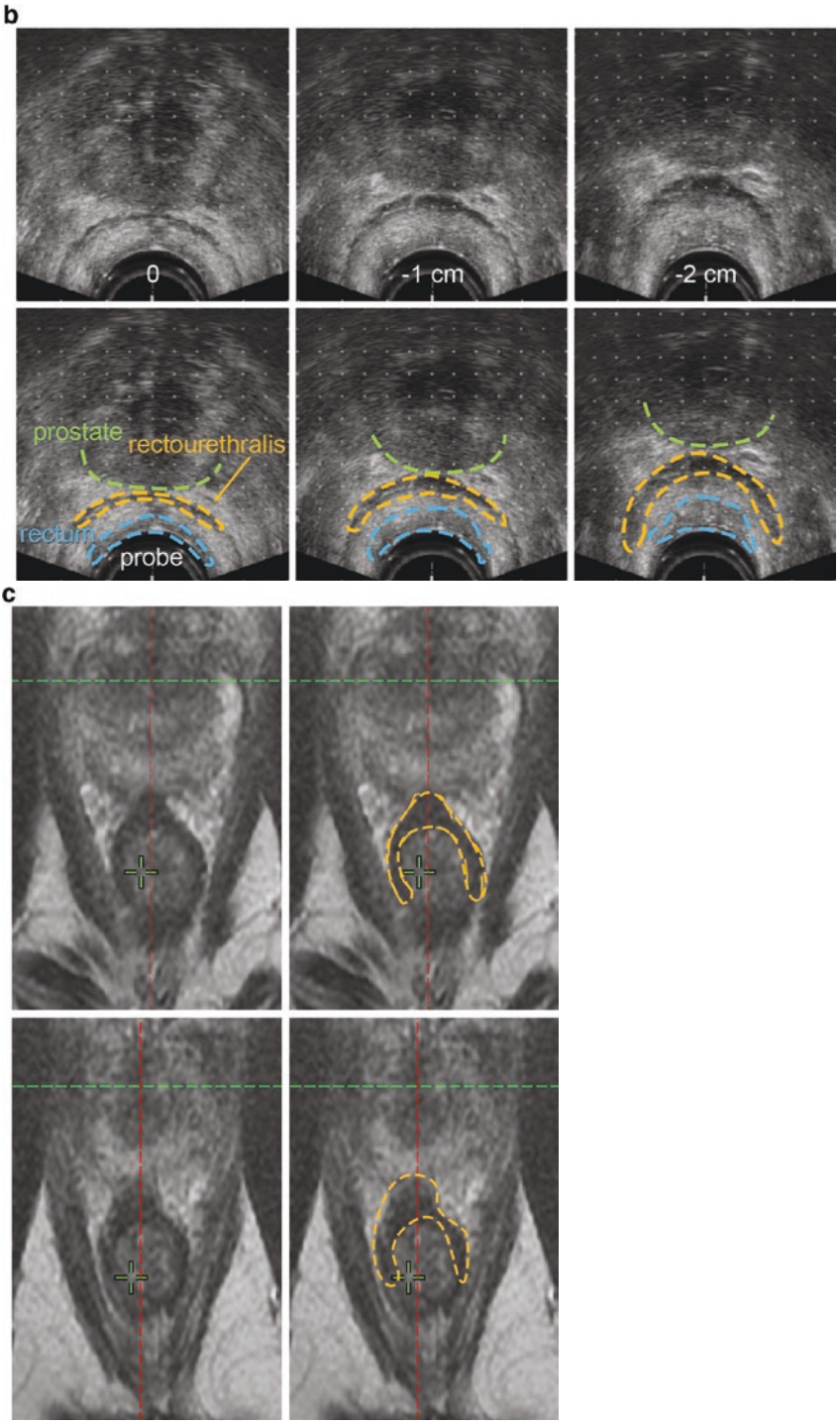

Fig. 2.12 (continued)

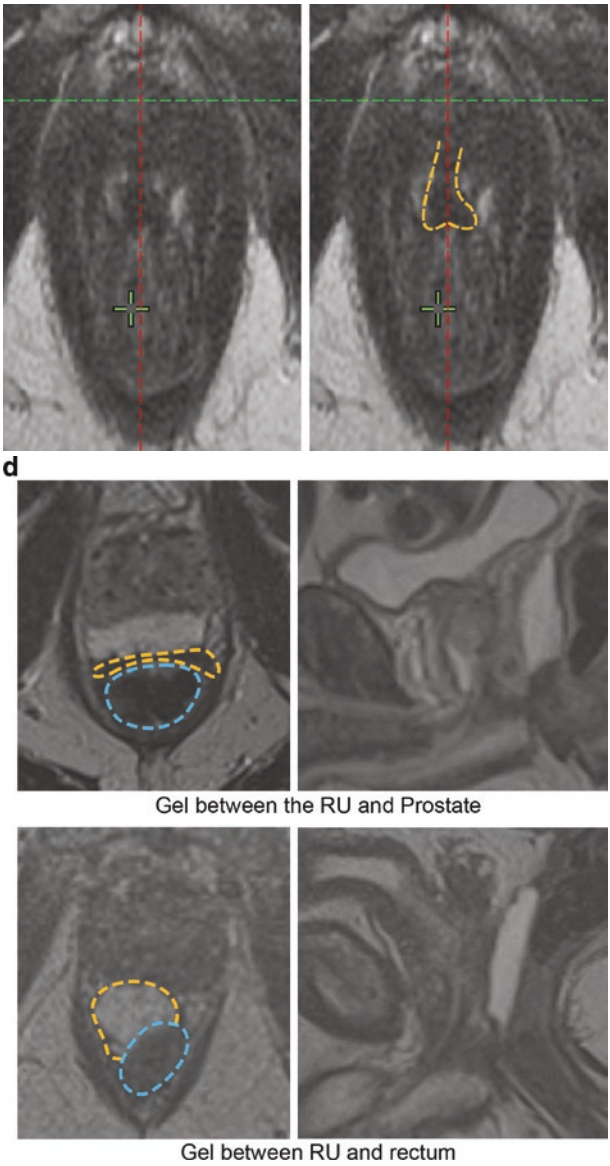

Fig. 2.12 (continued)

reported outcomes—90% reported the ability to be sexually active at 5 years [45]. Such success actually limits the capacity to implicate a critical target responsible.

– Critical distal target candidates include (1) cavernosal nerves coursing through the genitourinary diaphragm and over the penile bulb to terminate

on the corpus cavernosum, (2) the junction of terminal internal pudendal artery at the crura, (3) corpus cavernosa, (4) penile bulb (vascular and neural components course over the penile bulb), and (5) the internal pudendal artery itself, narrowing of which causes most erectile dysfunction in untreated men.
  - Profound erectile dysfunction after brachytherapy in which little or no dose is delivered to distal structures is proof that critical proximal structures can contribute to radiation-induced erectile dysfunction. Candidate structures are the neurovascular elements adjacent to the prostate and cavernosal nerves below the apex, and accessory pudendal arteries, common variants of the internal pudental arteries which course immediately adjacent to the prostate before terminating on the corpus cavernosa they supply.
- Previous preservation efforts emphasized erection sufficiency and climax but for some men loss of ejaculate is critical and they may characterize themselves as impotent, devastated in spite of preserved erections and climax. The next step in full sexual function preservation is ejaculate-sparing radiation.
  - The physiology of ejaculation is a complex, integrated process.
  - Radiation treatment may directly affect ejaculate-producing tissues such as seminal vesicles and prostate itself, or affect the transmission of ejaculate through the prostate via small ducts coursing to the verumontanum, or affect retrograde ejaculation transmission beyond the verumontanum due to bladder neck obstruction requiring alpha blockers.
  - Nerves adjacent to the prostate may also be affected by extreme doses for brachytherapy applications.
- The capacity to preserve full sexual function will depend on combining vessel sparing with additional strategies to limit loss of ejaculate. Examples of these include: bladder neck sparing so that alpha blockers are not necessary, preserving a portion of seminal vesicle to preserve ejaculate, avoiding direct implantation of nerve elements in brachytherapy procedures, and limiting or eliminating ADT. ADT are less critical to cure when intensive combined modality therapy (brachytherapy plus external beam RT) is used for earlier stages within the high risk categories.
  - In pilot studies, the feasibility to accomplish full sexual preservation in appropriate candidates has been demonstrated [45, 46].

2.4.8.2 Variant Anatomy

- The neurovascular elements are classically described as coursing posterolaterally to the prostate at 5 and 7 o'clock bilaterally, but significant variability in location and distribution of the neurovascular bundles has been shown [47, 48] (Fig. 2.13). This affects the ability to visualize the structures themselves and the degree to which they can be spared from treatment.

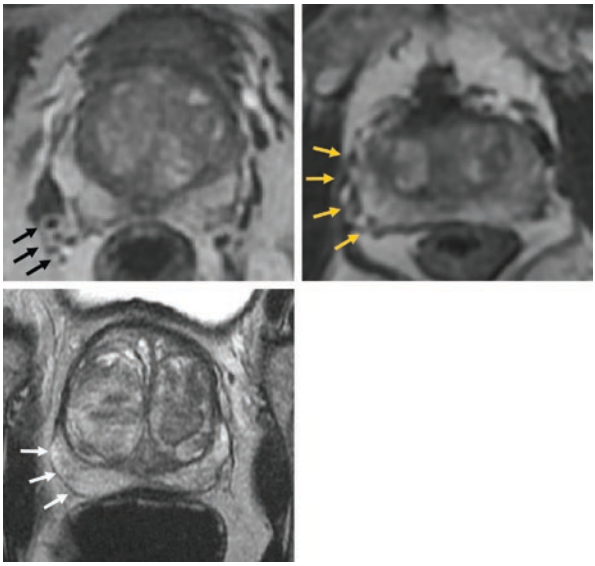

Fig. 2.13 Neurovascular elements (NVEs). Note the variation in nerve configuration. In 50–55% cases, a nerve bundle is present with a defined compartment posterior and lateral with visible elements within (top left). In 40–45% cases, the nerves are spread over the lateral and posterior surface, termed a plexus configuration (top right). In 5% cases, no elements are visible (bottom)

2.5 Imaging in Prostate Cancer Recurrence

- Detectable PSA >0.2 ng/mL following prostatectomy or rising PSA at least 2 ng/mL above the nadir following radiotherapy suggests residual or recurrent disease. Establishing the extent of disease in this setting is challenging, particularly when PSA remains relatively low.
- mpMRI and supersensitive PET scans can help to determine the specific location of a local recurrence and/or whether there is distant disease.

2.5.1 Post-prostatectomy

- In the setting of biochemical failure after prostatectomy, NCCN guidelines recommend consideration of chest imaging, local imaging with abdominopelvic CT or MRI and/or TRUS, and bone imaging with bone scan (and F-18 fluoride PET for equivocal findings) when clinical suspicion for bone metastases is high [11].
- CT and bone scan are of limited utility for determining the location of recurrent disease when post-prostatectomy biochemical failure is detected at low PSA levels. Salvage radiotherapy with uniform dose to the prostate bed with or without lymph node coverage is commonly recommended in this situation.

  - mpMRI is able to localize a site of recurrence in a substantial subset of these patients with sensitivity ranging from 60% to 99% across multiple studies [49–51]. One study found sensitivity of 76–82% for PSA <0.4, 60–73% for PSA 0.4–1.0, and 80–88% for PSA >1 [49], while another found sensitivity of 98% for a group with PSA 0.5–1.7 and 100% for a group with PSA 1.4–2.9 [50]. This information can potentially be used for target definition and/or dose intensification in salvage radiotherapy [52, 53].
- Consideration of advanced imaging with C-11 choline or F-18 fluciclovine PET: these scans are able to detect small volume disease in both the bones and soft tissue, by upregulated choline kinase cells in prostate cancer (choline) [54] or overexpression of amino-acid transport systems (fluciclovine) [55].
  - Choline PET has been shown to have a moderate overall sensitivity (32–65%) and specificity (40–90%), high positive predictive value (90–86%) and low negative predictive value (3–72%) for lymph node metastases [56, 57]. However, sensitivity and specificity for any recurrence has been reported as high as 89% for each in a meta-analysis [58].
  - Fluciclovine PET may be superior to choline PET in the setting of biochemical relapse with PPV 97% versus 90% in a prospective study [57], although more data is needed to make this assessment.
  - Sensitivity remains low for both modalities at lower PSA, with choline and fluciclovine PET at 14% and 21% for PSA <1 ng/mL, 29% and 29% for PSA 1–<2 ng/mL, 36% and 45% for PSA 2–<3, and 50% and 59% for PSA ≥3 in the same study [57].
- Imaging with Ga-68 prostate-specific membrane antigen (PSMA) has thus far demonstrated the greatest sensitivity with respect to disease detection at low PSA values, with superior detection rates compared to choline-based PET [59] although it has not yet obtained FDA approval. Ga-68 PSMA targets a transmembrane protein overexpressed in prostate cancer cells by 100–1000-fold depending on grade and stage of disease [54].
  - A recent meta-analysis showed detection rates of 33% (range 11–45%) and 46% (range 20–73%) for PSA <0.2 ng/mL and 0.2–0.49 ng/mL, respectively [60]. However, a small minority of patients with negative PSMA PET scans were found to have positive choline PET scans in another study [61].
- PET-labeled acetate and F-18 fluorodihydrotestosterone have also demonstrated some utility in the recurrent disease setting [62–64].

2.5.1.1 Variant Anatomy

- When evaluating post-prostatectomy MRI scans, it is important to understand the expected anatomical and imaging changes, such as fibrosis, inflammation, fat stranding, and artifacts due to surgical clips [65]. These anatomical changes are variable and can affect radiotherapy planning.
- External sphincter length after prostatectomy is highly variable and can clearly be seen on T2MRI (Fig. 2.14). When the external sphincter is long, it may be unnecessary to treat the full length, thus limiting late toxicity.

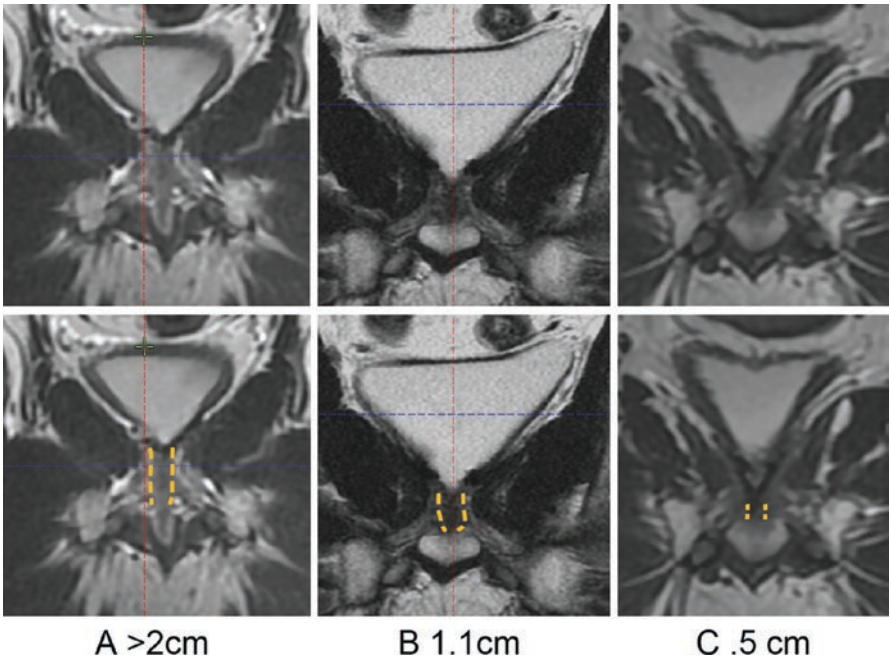

Fig. 2.14 Post-prostatectomy external sphincter (ES) variation. T2W MRI is invaluable in planning post-prostatectomy. While the DCE may actually define the recurrence, the ES length varies widely. In men with average to longer ES a portion can be spared. From left to right a long, medium, and short residual ES (dashed gold) is clearly defined on coronal T2MR

2.5.1.2 Functional Anatomy

- Recovery of continence and erectile function occurs over the course of approximately 1 year after prostatectomy. For patients who are candidates for ADT initiating this may allow further recovery time before initiating radiation.
- It is common practice to delay adjuvant or salvage radiotherapy until functional recovery has plateaued; however, there are no high-quality data to support the need for this practice (delay).
- mpMRI prior to initiating ADT may allow for localization of recurrent/residual disease prior to therapy response.

2.5.1.3 Tumor Anatomy

- Recurrent tumors exhibit similar imaging characteristics as primary tumors but can be more challenging to detect due to a lack of normal surrounding prostate and anatomical changes (Fig. 2.15).
- Functional MRI sequences (DCE, DWI) are critical in distinguishing between post-surgical changes and cancer recurrence.

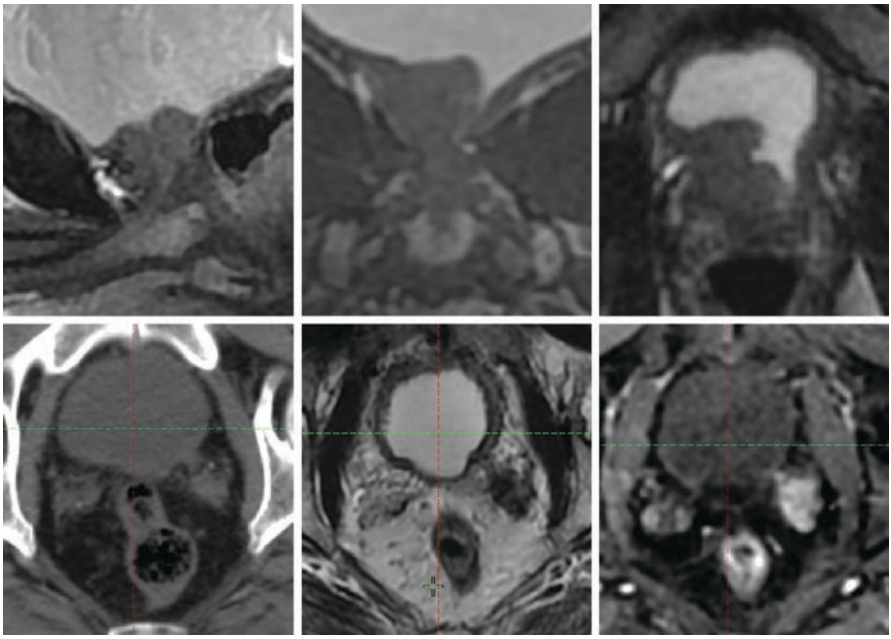

Fig. 2.15 Gross recurrence post-prostatectomy. MRI and PET are invaluable in defining gross recurrence post prostatectomy. In the upper panels, a gross recurrence mimics normal prostate on sagittal view, a regrowth presenting with a PSA of 24, without symptoms 14 years after surgery. In the lower panel, a lesion was palpable on physical exam and confirmed on DCE. Note how subtle the lesion appears on CT (lower left). Defining gross recurrence allows dose escalation and in recurrence post prior beam focal brachytherapy

- The vesicourethral anastomosis (VUA) typically appears as a low-signal ring of fibrosis on all sequences but can contain sites of higher signal on T2W scans due to the presence of inflammatory tissue.
- Tumors tend to be mildly hyperintense on T2W imaging and can be readily distinguished from fibrosis on DCE scans, by exhibiting rapid arterial enhancement and early washout in the venous phase.
- Hemorrhage and/or granulation tissue can enhance during the arterial phase but can usually be distinguished from tumor cells by a lack of restricted diffusion on DWI [65].

2.5.1.4 Dynamic Anatomy

- Bladder filling at the time of radiotherapy (readily seen on CT) helps to spare the bladder and bowel, but some men have limited ability to hold a full bladder after prostatectomy. Anticholinergic medication (such as Detrol) can be used in this situation, and occasionally penile clamps are necessary to achieve sufficient filling.

- Bowel can sometimes be seen filling the entire prostate fossa, limiting the ability to treat with standard salvage radiotherapy doses. Treating prone on a belly board is a potential solution to this problem.

2.5.2 Post-radiotherapy

- NCCN guidelines recommend bone imaging for all patients with recurrence after radiotherapy, but additional imaging only for those who are candidates for salvage local therapy to the prostate (initially T1–2, N0 or NX disease, life expectancy greater than 10 years and PSA <10 ng/mL) [11].
  - This includes chest imaging, prostate MRI, and consideration of abdominopelvic CT or MRI or fluciclovine PET scan (Fig. 2.16).
- mpMRI is a valuable tool for localizing recurrent disease, which is critical in the re-treatment process, as more focal therapy is commonly employed in this setting. However, interpretation of post-radiotherapy imaging is challenging due to treatment effect on the prostate and surrounding tissue (Fig. 2.16) and could be more so if brachytherapy seeds are present.

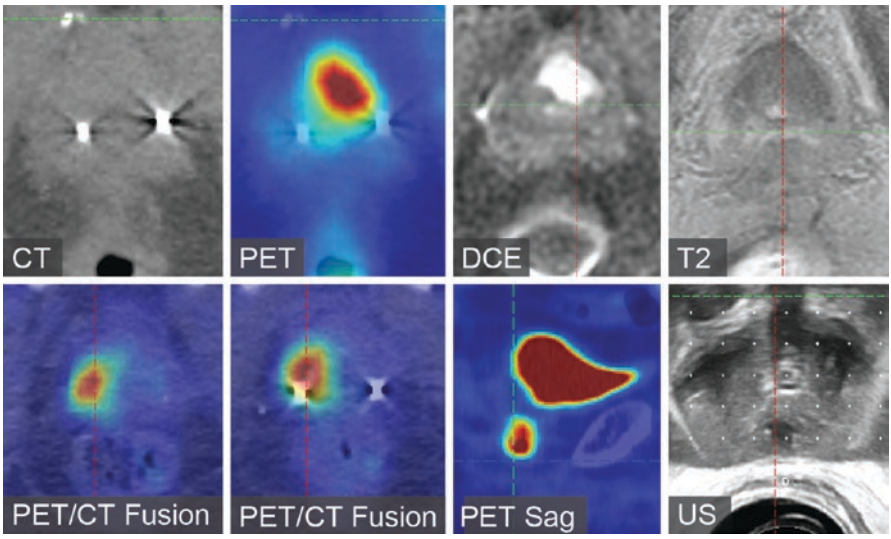

Fig. 2.16 Recurrence post radiation. Following radiation, the clear distinction of PZ (light) versus TZ (dark) on T2W is less apparent or abolished. This limits the utility of T2W in tumor recognition. DCE has a key role in such patients, recently joined by prostate-specific PET. In the upper panel, CT reveals no lesion, while ^{18}F fluciclovine PET and DCE clearly define the locations and extent. In the lower panel, a patient with a pacemaker/defibrillator was unable to arrange MRI in a timely fashion, but the PET clearly defined the extent of the recurrence. Note that no clear tumor is visible in the US panel at the level of fiducials

- Irradiated prostate appears diffusely hypointense on T2W scans, due to inflammation, glandular atrophy, fibrosis, and volume shrinkage [66]. This results in a loss of zonal demarcation that will have been apparent on pre-treatment scans.
- Comparison with pre-treatment MRI is valuable, as recurrence most commonly occurs at the site of the original primary tumor. Even when this is available, distinguishing between recurrence and normal irradiated tissue remains difficult due to the reduced contrast and signal intensity differences between these tissues on T2W [66].
- Multiple studies have shown the benefits of including DCE and DWI for detecting local prostate cancer recurrence after radiotherapy [67–69]. Imaging characteristics of recurrent tumors are similar to those of primary disease, with rapid focal enhancement and early washout on DCE and restricted diffusion on DWI (hypointense on ADC maps).
- Ultrasensitive PET scans are particularly helpful in localizing recurrent disease when MRI imaging findings are not definitive. Choline PET was found to have 95% sensitivity and 73% specificity for recurrence in the post-RT setting [70]. PET can also be invaluable for diagnosing metastatic disease in this setting, as noted in Sect. 2.5.1 and shown in Fig. 2.17.

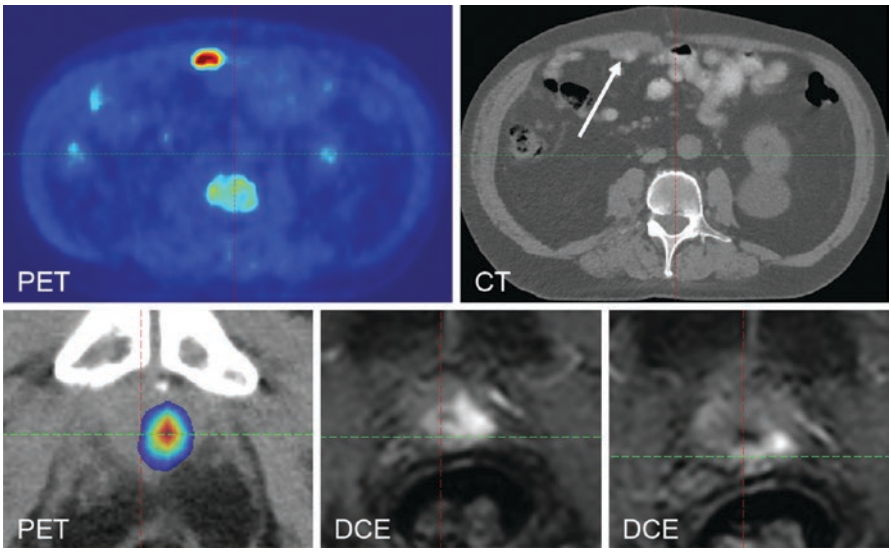

Fig. 2.17 Recurrence after post-op radiation. PET is invaluable in defining recurrence after post-op radiation. In the upper panel, a man with rising PSA and negative bone scan and CT AP had a positive ^{68}GA PSMA PET in the abdominal wall and small nodules throughout the peritoneum. In all likelihood, this unusual distribution represented surgical dissemination to a port used in robotic prostatectomy. In the lower panel, a recurrence was localized by PET at the anatomic site but largely within the bladder wall, most clearly defined on DCE

2.6 Summary

- Contemporary prostate cancer imaging offers both tremendous opportunity and challenge for radiation treatment planning. The opportunity: 100% local control, full genitourinary, gastrointestinal, and sexual function preservation, with reduced acute and chronic toxicity. The challenge: achieving expertise in variant, functional, dynamic, and tumor anatomy and the integration of radiologic expertise into radiation oncology workflow. In this chapter, we have introduced the opportunity and challenges to fulfill the modern goal of successful therapy; cure with preserved quality of life.

References

1. Lin A, Kim HM, Terrell JE, Dawson LA, Ship JA, Eisbruch A (2003) Quality of life after parotid-sparing IMRT for head-and-neck cancer: a prospective longitudinal study. Int J Radiat Oncol Biol Phys 57(1):61–70
2. de Rooij M, Hamoen EH, Witjes JA, Barentsz JO, Rovers MM (2016) Accuracy of magnetic resonance imaging for local staging of prostate cancer: a diagnostic meta-analysis. Eur Urol 70(2):233–245
3. Gaunay G, Patel V, Shah P, Moreira D, Hall SJ, Vira MA et al (2017) Role of multi-parametric MRI of the prostate for screening and staging: experience with over 1500 cases. Asian J Urol 4(1):68–74
4. Futterer JJ, Briganti A, De Visschere P, Emberton M, Giannarini G, Kirkham A et al (2015) Can clinically significant prostate cancer be detected with multiparametric magnetic resonance imaging? A systematic review of the literature. Eur Urol 68(6):1045–1053
5. Wysock JS, Mendhiratta N, Zattoni F, Meng X, Bjurlin M, Huang WC et al (2016) Predictive value of negative 3T multiparametric magnetic resonance imaging of the prostate on 12-core biopsy results. BJU Int 118(4):515–520
6. Itatani R, Namimoto T, Atsuji S, Katahira K, Morishita S, Kitani K et al (2014) Negative predictive value of multiparametric MRI for prostate cancer detection: outcome of 5-year follow-up in men with negative findings on initial MRI studies. Eur J Radiol 83(10):1740–1745
7. Sherrer RL, Glaser ZA, Gordetsky JB, Nix JW, Porter KK, Rais-Bahrami S (2019) Comparison of biparametric MRI to full multiparametric MRI for detection of clinically significant prostate cancer. Prostate Cancer Prostatic Dis 22(2):331–336
8. Shoag J, Mittal S, Halpern JA, Scherr D, Hu JC, Barbieri CE (2016) Lethal prostate cancer in the PLCO cancer screening trial. Eur Urol 70(1):2–5
9. Kasivisvanathan V, Rannikko AS, Borghi M, Panebianco V, Mynderse LA, Vaarala MH et al (2018) MRI-targeted or standard biopsy for prostate-cancer diagnosis. N Engl J Med 378(19):1767–1777
10. Kuhl CK, Bruhn R, Krämer N, Nebelung S, Heidenreich A, Schrading S (2017) Abbreviated biparametric prostate MR imaging in men with elevated prostate-specific antigen. Radiology 285(2):493–505
11. Hawkins PG, Lee JY, Mao Y, Li P, Green M, Worden FP et al (2018) Sparing all salivary glands with IMRT for head and neck cancer: longitudinal study of patient-reported xerostomia and head-and-neck quality of life. Radiother Oncol 126(1):68–74
12. Wondergem M, van der Zant FM, van der Ploeg T, Knol RJ (2013) A literature review of 18F-fluoride PET/CT and 18F-choline or 11C-choline PET/CT for detection of bone metastases in patients with prostate cancer. Nucl Med Commun 34(10):935–945

13. Parker CC, James ND, Brawley CD, Clarke NW, Hoyle AP, Ali A et al (2018) Radiotherapy to the primary tumour for newly diagnosed, metastatic prostate cancer (STAMPEDE): a randomised controlled phase 3 trial. Lancet 392(10162):2353–2366
14. Gravis G, Boher JM, Chen YH, Liu G, Fizazi K, Carducci MA et al (2018) Burden of metastatic castrate naive prostate cancer patients, to identify men more likely to benefit from early docetaxel: further analyses of CHAARTED and GETUG-AFU15 studies. Eur Urol 73(6):847–855
15. Lecouvet FE, Oprea-Lager DE, Liu Y, Ost P, Bidaut L, Collette L et al (2018) Use of modern imaging methods to facilitate trials of metastasis-directed therapy for oligometastatic disease in prostate cancer: a consensus recommendation from the EORTC Imaging Group. Lancet Oncol 19(10):e534–ee45
16. Gandaglia G, Briganti A, Clarke N, Karnes RJ, Graefen M, Ost P et al (2017) Adjuvant and salvage radiotherapy after radical prostatectomy in prostate cancer patients. Eur Urol 72(5):689–709
17. Swanson GP, Riggs M, Hermans M (2007) Pathologic findings at radical prostatectomy: risk factors for failure and death. Urol Oncol 25(2):110–114
18. Mungovan SF, Sandhu JS, Akin O, Smart NA, Graham PL, Patel MI (2017) Preoperative membranous urethral length measurement and continence recovery following radical prostatectomy: a systematic review and meta-analysis. Eur Urol 71(3):368–378
19. Savera AT, Kaul S, Badani K, Stark AT, Shah NL, Menon M (2006) Robotic radical prostatectomy with the "Veil of Aphrodite" technique: histologic evidence of enhanced nerve sparing. Eur Urol 49(6):1065–1073. discussion 73–4
20. McLaughlin PW, Evans C, Feng M, Narayana V (2010) Radiographic and anatomic basis for prostate contouring errors and methods to improve prostate contouring accuracy. Int J Radiat Oncol Biol Phys 76(2):369–378
21. Chung E, Stenmark MH, Evans C, Narayana V, McLaughlin PW (2012) Expansion/de-expansion tool to quantify the accuracy of prostate contours. Int J Radiat Oncol Biol Phys 83(1):33–37
22. Gao Z, Wilkins D, Eapen L, Morash C, Wassef Y, Gerig L (2007) A study of prostate delineation referenced against a gold standard created from the visible human data. Radiother Oncol 85(2):239–246
23. Rosenkrantz AB, Taneja SS (2014) Radiologist, be aware: ten pitfalls that confound the interpretation of multiparametric prostate MRI. AJR Am J Roentgenol 202(1):109–120
24. Venkatesan AM, Stafford RJ, Duran C, Soni PD, Berlin A, McLaughlin PW (2017) Prostate magnetic resonance imaging for brachytherapists: anatomy and technique. Brachytherapy 16(4):679–687
25. Chen M, Hricak H, Kalbhen CL, Kurhanewicz J, Vigneron DB, Weiss JM et al (1996) Hormonal ablation of prostatic cancer: effects on prostate morphology, tumor detection, and staging by endorectal coil MR imaging. Am J Roentgenol 166(5):1157–1163
26. Zechmann CM, Simpfendorfer T, Giesel FL, Zamecnik P, Thieke C, Hielscher T et al (2010) Comparison of peripheral zone and central gland volume in patients undergoing intensity-modulated radiotherapy. J Comput Assist Tomogr 34(5):739–745
27. Soni PD, Yao B, Evans C, Abugharib AE, Narayana V, McLaughlin PW (2016) The brachytherapy "Bermuda triangle": a potential space with important implications for LDR and HDR prostate brachytherapy. Brachytherapy 15:S175–S1S6
28. Soni PD, Berlin A, Venkatesan AM, McLaughlin PW (2017) Magnetic resonance imaging-guided functional anatomy approach to prostate brachytherapy. Brachytherapy 16(4):698–714
29. Liss A, Murgic J, Evans C, Narayana V, McLaughlin P (2013) Variation in external sphincter extension within and beyond the prostate: implications from MRI-based post implant segmental dosimetry. Brachytherapy 12:S33
30. Soh S, Arakawa A, Suyama K, Scardino P, Wheeler T (1998) The prognosis of patients with seminal vesicle involvement (SVI) depends upon the level of extraprostatic extension (EPE). J Urol 159:296

31. Partin AW, Yoo J, Carter HB, Pearson JD, Chan DW, Epstein JI et al (1993) The use of prostate specific antigen, clinical stage and Gleason score to predict pathological stage in men with localized prostate cancer. J Urol 150(1):110–114
32. Grivas N, Hinnen K, de Jong J, Heemsbergen W, Moonen L, Witteveen T et al (2018) Seminal vesicle invasion on multi-parametric magnetic resonance imaging: correlation with histopathology. Eur J Radiol 98:107–112
33. Kestin L, Goldstein N, Vicini F, Yan D, Korman H, Martinez A (2002) Treatment of prostate cancer with radiotherapy: should the entire seminal vesicles be included in the clinical target volume? Int J Radiat Oncol Biol Phys 54(3):686–697
34. Samaratunga H, Samaratunga D, Perry-Keene J, Adamson M, Yaxley J, Delahunt B (2010) Distal seminal vesicle invasion by prostate adenocarcinoma does not occur in isolation of proximal seminal vesicle invasion or lymphovascular infiltration. Pathology 42(4):330–333
35. Silva RC, Sasse AD, Matheus WE, Ferreira U (2013) Magnetic resonance image in the diagnosis and evaluation of extra-prostatic extension and involvement of seminal vesicles of prostate cancer: a systematic review of literature and meta-analysis. Int Braz J Urol 39:155–166
36. Radtke JP, Hadaschik BA, Wolf MB, Freitag MT, Schwab C, Alt C et al (2015) The impact of magnetic resonance imaging on prediction of extraprostatic extension and prostatectomy outcome in patients with low-, intermediate- and high-risk prostate cancer: try to find a standard. J Endourol 29(12):1396–1405
37. Engelbrecht MR, Jager GJ, Laheij RJ, Verbeek AL, van Lier H, Barentsz JO (2002) Local staging of prostate cancer using magnetic resonance imaging: a meta-analysis. Eur Radiol 12(9):2294–2302
38. Morlacco A, Sharma V, Viers BR, Rangel LJ, Carlson RE, Froemming AT et al (2017) The incremental role of magnetic resonance imaging for prostate cancer staging before radical prostatectomy. Eur Urol 71(5):701–704
39. Dess R, Evans CA, Narayana V, Abugharib AE, McLaughlin PW (2016) Bladder neck variants: MRI versus ultrasound definition. Brachytherapy 15:S195–S1S6
40. McNeal JE, Redwine EA, Freiha FS, Stamey TA (1988) Zonal distribution of prostatic adenocarcinoma. Correlation with histologic pattern and direction of spread. Am J Surg Pathol 12(12):897–906
41. Walsh PC (1998) Anatomic radical prostatectomy: evolution of the surgical technique. J Urol 160(6 Pt 2):2418–2424
42. Ficarra V, Novara G, Ahlering TE, Costello A, Eastham JA, Graefen M et al (2012) Systematic review and meta-analysis of studies reporting potency rates after robot-assisted radical prostatectomy. Eur Urol 62(3):418–430
43. Merrick GS, Butler WM, Galbreath RW, Stipetich RL, Abel LJ, Lief JH (2002) Erectile function after permanent prostate brachytherapy. Int J Radiat Oncol Biol Phys 52(4):893–902
44. Merrick GS, Butler WM, Wallner KE, Galbreath RW, Anderson RL, Kurko BS et al (2005) Erectile function after prostate brachytherapy. Int J Radiat Oncol Biol Phys 62(2):437–447
45. Lee JY, Spratt DE, Liss AL, McLaughlin PW (2016) Vessel-sparing radiation and functional anatomy-based preservation for erectile function after prostate radiotherapy. Lancet Oncol 17(5):e198–e208
46. Spratt DE, Lee JY, Dess RT, Narayana V, Evans C, Liss A et al (2017) Vessel-sparing radiotherapy for localized prostate cancer to preserve erectile function: a single-arm phase 2 trial. Eur Urol 72(4):617–624
47. Liss A, Zhou J, Evans C, Murgic J, Narayana V, Hamstra DA et al (2014) Anatomic variability of the neurovascular elements defined by MRI. Brachytherapy 13:S42–SS3
48. Lee SB, Hong SK, Choe G, Lee SE (2008) Periprostatic distribution of nerves in specimens from non-nerve-sparing radical retropubic prostatectomy. Urology 72(4):878–881
49. Kitajima K, Hartman RP, Froemming AT, Hagen CE, Takahashi N, Kawashima A (2015) Detection of local recurrence of prostate cancer after radical prostatectomy using endorectal coil MRI at 3 T: addition of DWI and dynamic contrast enhancement to T2-weighted MRI. AJR Am J Roentgenol 205(4):807–816

50. Panebianco V, Barchetti F, Sciarra A, Musio D, Forte V, Gentile V et al (2013) Prostate cancer recurrence after radical prostatectomy: the role of 3-T diffusion imaging in multi-parametric magnetic resonance imaging. Eur Radiol 23(6):1745–1752
51. Sella T, Schwartz LH, Swindle PW, Onyebuchi CN, Scardino PT, Scher HI et al (2004) Suspected local recurrence after radical prostatectomy: endorectal coil MR imaging. Radiology 231(2):379–385
52. Park JS, Park W, Pyo HR, Park BK, Park SY, Choi HY et al (2014) Suggestion for the prostatic fossa clinical target volume in adjuvant or salvage radiotherapy after a radical prostatectomy. Radiother Oncol 110(2):240–244
53. Miralbell R, Vees H, Lozano J, Khan H, Mollà M, Hidalgo A et al (2007) Endorectal MRI assessment of local relapse after surgery for prostate cancer: a model to define treatment field guidelines for adjuvant radiotherapy in patients at high risk for local failure. Int J Radiat Oncol Biol Phys 67(2):356–361
54. Moghanaki D, Turkbey B, Vapiwala N, Ehdaie B, Frank SJ, McLaughlin PW et al (2017) Advances in prostate cancer magnetic resonance imaging and positron emission tomography-computed tomography for staging and radiotherapy treatment planning. Semin Radiat Oncol 27(1):21–33
55. Okudaira H, Nakanishi T, Oka S, Kobayashi M, Tamagami H, Schuster DM et al (2013) Kinetic analyses of trans-1-amino-3-[18F]fluorocyclobutanecarboxylic acid transport in Xenopus laevis oocytes expressing human ASCT2 and SNAT2. Nucl Med Biol 40(5):670–675
56. Scattoni V, Picchio M, Suardi N, Messa C, Freschi M, Roscigno M et al (2007) Detection of lymph-node metastases with integrated [11C]choline PET/CT in patients with PSA failure after radical retropubic prostatectomy: results confirmed by open pelvic-retroperitoneal lymphadenectomy. Eur Urol 52(2):423–429
57. Nanni C, Zanoni L, Pultrone C, Schiavina R, Brunocilla E, Lodi F et al (2016) (18)F-FACBC (anti1-amino-3-(18)F-fluorocyclobutane-1-carboxylic acid) versus (11)C-choline PET/CT in prostate cancer relapse: results of a prospective trial. Eur J Nucl Med Mol Imaging 43(9):1601–1610
58. Fanti S, Minozzi S, Castellucci P, Balduzzi S, Herrmann K, Krause BJ et al (2016) PET/CT with 11C-choline for evaluation of prostate cancer patients with biochemical recurrence: meta-analysis and critical review of available data. Eur J Nucl Med Mol Imaging 43(1):55–69
59. Perera M, Papa N, Christidis D, Wetherell D, Hofman MS, Murphy DG et al (2016) Sensitivity, specificity, and predictors of positive (68)Ga-prostate-specific membrane antigen positron emission tomography in advanced prostate cancer: a systematic review and meta-analysis. Eur Urol 70(6):926–937
60. Perera M, Papa N, Roberts M, Williams M, Udovicich C, Vela I et al (2020) Gallium-68 prostate-specific membrane antigen positron emission tomography in advanced prostate cancer—updated diagnostic utility, sensitivity, specificity, and distribution of prostate-specific membrane antigen-avid lesions: a systematic review and meta-analysis. Eur Urol 77(4):403–417
61. Schwenck J, Rempp H, Reischl G, Kruck S, Stenzl A, Nikolaou K et al (2017) Comparison of 68Ga-labelled PSMA-11 and 11C-choline in the detection of prostate cancer metastases by PET/CT. Eur J Nucl Med Mol Imaging 44(1):92–101
62. Mohsen B, Giorgio T, Rasoul ZS, Werner L, Ali GR, Reza DK et al (2013) Application of C-11-acetate positron-emission tomography (PET) imaging in prostate cancer: systematic review and meta-analysis of the literature. BJU Int 112(8):1062–1072
63. Soyka JD, Muster MA, Schmid DT, Seifert B, Schick U, Miralbell R et al (2012) Clinical impact of 18F-choline PET/CT in patients with recurrent prostate cancer. Eur J Nucl Med Mol Imaging 39(6):936–943
64. Dehdashti F, Picus J, Michalski JM, Dence CS, Siegel BA, Katzenellenbogen JA et al (2005) Positron tomographic assessment of androgen receptors in prostatic carcinoma. Eur J Nucl Med Mol Imaging 32(3):344–350
65. Gaur S, Turkbey B (2018) Prostate MR imaging for post-treatment evaluation and recurrence. Radiol Clin N Am 56(2):263–275

66. Venkatesan AM, Stafford RJ, Duran C, Soni PD, Berlin A, McLaughlin PW (2017) Prostate magnetic resonance imaging for brachytherapists: diagnosis, imaging pitfalls, and post-therapy assessment. Brachytherapy 16(4):688–697
67. Kim CK, Park BK, Park W, Kim SS (2010) Prostate MR imaging at 3T using a phased-arrayed coil in predicting locally recurrent prostate cancer after radiation therapy: preliminary experience. Abdom Imaging 35(2):246–252
68. Haider MA, Chung P, Sweet J, Toi A, Jhaveri K, Menard C et al (2008) Dynamic contrast-enhanced magnetic resonance imaging for localization of recurrent prostate cancer after external beam radiotherapy. Int J Radiat Oncol Biol Phys 70(2):425–430
69. Rouviere O, Valette O, Grivolat S, Colin-Pangaud C, Bouvier R, Chapelon JY et al (2004) Recurrent prostate cancer after external beam radiotherapy: value of contrast-enhanced dynamic MRI in localizing intraprostatic tumor—correlation with biopsy findings. Urology 63(5):922–927
70. Parker WP, Davis BJ, Park SS, Olivier KR, Choo R, Nathan MA et al (2017) Identification of site-specific recurrence following primary radiation therapy for prostate cancer using C-11 choline positron emission tomography/computed tomography: a nomogram for predicting extrapelvic disease. Eur Urol 71(3):340–348